Elastic flexibility, fast-ion conduction, boson and floppy modes in AgPO$_3$–AgI glasses

Deassy I Novita[1], **P Boolchand**[1], **M Malki**[2,3] **and Matthieu Micoulaut**[4]

[1] Department of Electrical and Computer Engineering, University of Cincinnati, Cincinnati, OH 45221-0030, USA

[2] CNRS, UPR 3079 CEMHTI, 1D avenue de la Recherche Scientifique, F-45071 Orléans Cedex 2, France

[3] Polytech'Orléans—Université d'Orléans, 8 rue Léonard de Vinci, F-45072 Orléans, France

[4] Laboratoire de Physique Theorique de la Matiere Condensée, Université Pierre et Marie Curie, BP 121, 4 Place Jussieu, F-75252 Paris Cedex 05, France

Abstract

Raman scattering, IR reflectance and modulated-DSC measurements are performed on specifically prepared dry $(AgI)_x(AgPO_3)_{1-x}$ glasses over a wide range of compositions $0\% < x < 60\%$. A reversibility window is observed in the $9.5\% < x < 37.8\%$ range, which fixes the elastically rigid but unstressed regime also known as the intermediate phase. Glass compositions at $x < 9.5\%$ are stressed-rigid, while those at $x > 37.8\%$ are elastically flexible. Raman optical elasticity power laws, trends in the nature of the glass transition endotherms, corroborate the three elastic phase assignments. Ionic conductivities reveal a step-like increase when glasses become stress-free at $x > x_c(1) = 9.5\%$ and a logarithmic increase in conductivity ($\sigma \sim (x - x_c(2))^\mu$) once they become flexible at $x > x_c(2) = 37.8\%$ with a power law $\mu = 1.78$. The power law is consistent with percolation of 3D filamentary conduction pathways. Traces of water doping lower T_g and narrow the reversibility window, and can also completely collapse it. Ideas on network flexibility promoting ion conduction are in harmony with the unified approach of Ingram *et al* (2008 *J. Phys. Chem.* B **112** 859), who have emphasized the similarity of process compliance or elasticity relating to ion transport and structural relaxation in decoupled systems. Boson mode frequency and scattering strength display thresholds that coincide with the two elastic phase boundaries. In particular, the scattering strength of the boson mode increases almost linearly with glass composition x, with a slope that tracks the *floppy mode fraction* as a function of mean coordination number r predicted by mean-field rigidity theory. These data suggest that the excess low frequency vibrations contributing to the boson mode in flexible glasses come largely from *floppy modes*.

(Some figures in this article are in colour only in the electronic version)

1. Introduction

Solid electrolyte glasses usually consist of alloys of a base oxide or chalcogenide glass with a solid electrolyte additive. In many instances the base and additive components form homogeneous alloy glasses over a wide range of compositions [1–4]. In other instances, phase separation occurs as a solid electrolyte phase segregates either on a nanoscale [5] or a microscale [3, 6]. In homogeneous glasses, ions such as Ag$^+$ or Li$^+$ diffuse by hopping and contribute to high ionic conductivity with increasing solid electrolyte content [1–4]. Substantial progress in modeling ion transport in solid electrolyte glasses has taken place over the past two decades [7–14]. In spite of these developments, we are still not in a position to reliably identify the mechanisms that control fast-ion transport at present so as to optimize the highest conductivity achievable. It is not clear what aspects of local and intermediate range structures of a glass network, if any, control ion transport.

It is generally believed [8, 9, 15, 16] that in solid electrolyte glasses physical processes associated with ion transport and network structure are *decoupled*. For example, the ratio (R_τ) of structural ($\tau_s \sim 10^2$ s) to conductivity ($\tau_\sigma \sim 10^{-10}$ s) relaxation times near the glass transition temperature (T_g) is of the order of $R_\tau \sim 10^{12}$. On the other hand, in polymer electrolytes such as polyalkylene oxides, R_τ values of nearly 1 or even less than 1 have been observed [15, 17]. In these *coupled* systems, clearly a reverse circumstance must prevail, namely ion hopping and network structure relaxation must be closely tied to each other.

Recently Ingram *et al* [18] have investigated the glassy electrolyte system $(AgI)_{50}(Ag_2O)_{25}(MoO_3)_{25}$ in conductivity and pressure-DSC experiments. The Ag-iodomolybdate is an example of a decoupled solid electrolyte glass system. The activation energy (ΔE_A) and the activated volume (ΔV_A) are estimated from conductivity measurements [19–21]. Pressure-DSC measurements are used to obtain the moduli for structural relaxation M_s from a pressure dependence measurement of the fictive temperature T_f. Ingram *et al* suggest that moduli for conductivity relaxation or structural relaxation can be defined as the ratio of activation energy (ΔE_A) and activated volume (ΔV_A):

$$M = \Delta E_A / \Delta V_A. \tag{1}$$

For the case of silver iodomolybdate they find conductivity (σ) and structure (s) relaxation processes, to yield the *same moduli*, i.e. $M_\sigma = M_s$. They conclude that basic interactions that control ion transport and network structure relaxation in decoupled (glasses) systems are essentially the *same*. Ingram *et al* [18] identify the ratio M as representing a 'process' modulus and find decoupled systems like electrolyte glasses possess larger moduli than coupled systems like polymer electrolytes. In glassy electrolytes, the activated volumes, and therefore activated energies, are much smaller for ion transport than for structural relaxation ones, leading to much shorter relaxation times in the former processes. For example, Ingram *et al* [18] estimate the activated volume for conductivity to be about 2.3 cc/mole, while that for structure relaxation at about 200 cc/mole, almost two orders of magnitude larger. These observations are striking and bring *decoupled* and *coupled* electrolytes under a common platform. These ideas suggest that very similar elementary processes are operating over a wide range of relaxation times in electrolytes.

In the present work we have examined the $(AgI)_x$ $(AgPO_3)_{1-x}$ solid electrolyte glass system in a variety of experiments including modulated-DSC, Raman scattering and IR reflectance, AC conductivity and molar volume experiments as a function of glass composition x, paying particular attention to the handling of precursors in the synthesis of samples. A brief version of the present work has appeared recently [1]. This particular electrolyte glass has been widely examined in the past by more than a dozen groups [7, 12, 22–33]. Our experiments reveal that traces of water intimately affect network structure, glass transition temperatures [34], network elasticity, ion transport [1] and, in general, the physical behavior of these glasses much more so than hitherto recognized [35]. In dry samples, we observe the *intrinsic* elastic behavior of these glasses, which displays

three distinct elastic phases [1] as a function of increasing AgI content x; a *stressed-rigid phase* in the $0\% < x < 9.5\%$ range, an *intermediate phase* in the $9.5\% < x < 37.8\%$ range and a *flexible phase* in the $37.8\% < x < 54\%$ range. The underlying elastic phase boundaries are quite sensitive to the water content of glasses. At higher concentrations of AgI ($x > 54\%$) glasses segregate into AgI-rich regions. Ionic conductivities of dry samples, examined as a function of increasing AgI concentration, display an increase that occurs in *two* step-like fashion; one of these steps occurs near $x \sim 9.5\%$ once glasses become stress-free and the second step occurs near $x \sim 37.8\%$ when glasses become elastically flexible. In the flexible phase ($x > 37.8\%$), ionic conductivities increase as a power law as a function of composition. These data suggest the existence of characteristic conducting pathways that apparently percolate in 3D once the network structure becomes flexible at $x > 37.8\%$. Our findings are in harmony with the notion that rigidity and flexibility of the glass network structure are closely related to ion transport.

The observation of the three elastic phases in a solid electrolyte glass system is a significant finding. Such elastic phases were observed earlier in covalent glasses [36] and in oxide glasses [37]. To the best of our knowledge, observation of these phases in a fast-ion conducting glass is reported in this work for the first time. These results suggest that classification of network glasses into three elastic phases based on their connectivity appears to be a generic behavior. It is now feasible to identify the elastic phase a glass composition belongs to by examining the nature of the glass transition in modulated-differential scanning calorimetry (m-DSC).

This paper is organized as follows. In section 2 we present experimental results. In section 3 we present some theoretical considerations in enumeration of Lagrangian constraints in $AgPO_3$ and AgI. A discussion of the present results follows in section 4. A summary of conclusions appears in section 5.

2. Experimental details

2.1. Synthesis

Set A. Dry $(AgPO_3)_{1-x}(AgI)_x$ glasses were synthesized using 99.9% Ag_3PO_4 (Alpha Aesar Inc.), 99.5% P_2O_5 (Fischer Scientific Inc.) and 99.99%AgI (Alpha Aesar Inc.) as the starting materials. The bottles containing the starting materials from the supplier were left to stand in a nitrogen-gas-purged glove box [34] (relative humidity $\ll 1/5\%$) overnight prior to opening them. The starting materials were weighed in the desired proportion and thoroughly mixed in an alumina crucible with all handling performed [34] in a glove box (Vacuum Atmospheres model HE-493/MO-5) with a relative humidity much less than $1/5\%$. Mixtures were then transferred to a box furnace held at 125 °C in a chemical hood purged by laboratory air, and heated at 100 °C h^{-1} to 700 °C. Melts were equilibrated overnight and then quenched over steel plates. Once synthesized, glass samples were encapsulated in evacuated (10^{-7} Torr) pyrex tubing for long term storage.

Set B. The principal difference in processing between set B and set A was the starting material Ag_3PO_4. The bottles containing the starting materials were opened in the
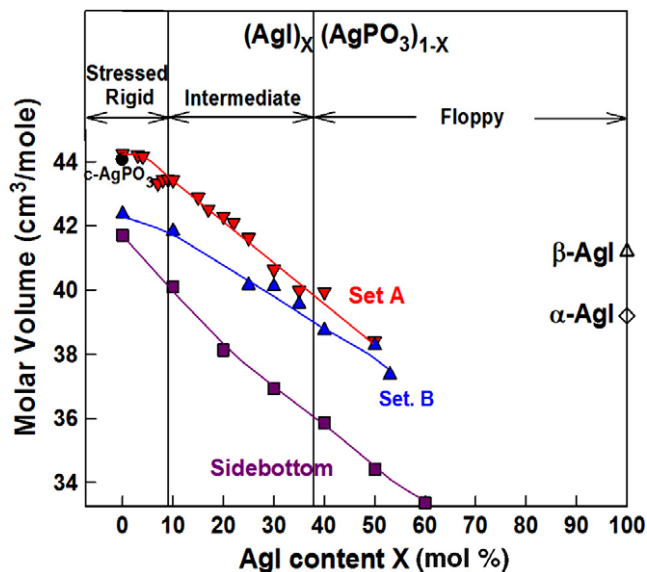
Figure 1. Variations in molar volume $V_M(x)$ in set A (dry: ▼), set B (wet: ▲) $(AgI)_x(AgPO_3)_{1-x}$ glasses synthesized in the present work and those reported by Sidebottom [26] (■).
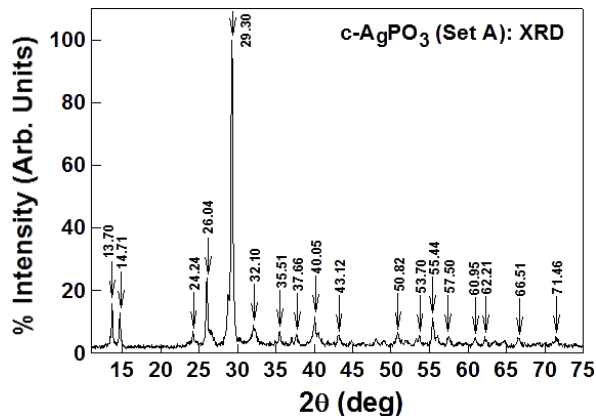

Figure 2. X-ray powder diffraction pattern of crystalline $AgPO_3$ glass sample in set A. Note that the most intense Bragg peak in XRD results of our sample occurs at $2\Theta = 29.30°$. It is shifted to a lower value than the published result ($2\Theta = 31.67°$) from the Joint Committee on Powder Diffraction Standards (JCPDS) [40] data file # 11-0640.

laboratory ambient environment for a short time in the early phase of our experiments. This procedure contaminated the starting material by introducing traces of water from the laboratory ambient environment. Subsequently the bottles were transferred to the glove bag with a relative humidity ~5% and all handling of the materials were performed in there. Other processing steps were identical to the ones used in synthesizing set A.

Crystalline AgPO₃. A sample of dry $AgPO_3$ (set A) was crystallized by heating to 360 °C and held at that temperature for 12 h, followed by cooling to room temperature over approximately 4 h. The crystalline nature of the sample was confirmed in x-ray diffraction experiments (see below). Molar volume of the crystalline sample was also measured and compared to the starting glass sample (see below).

2.2. Molar volumes

The molar volume of samples was established from mass densities established using Archimedes' principle. In a measurement, a glass sample piece (100 mg or more in size) was mounted on a thin quartz fiber attached to a Mettler Toledo physical balance model B154 and weights recorded in air and in pure ethyl alcohol (AAPER Alcohol and Chemical Co.). A 1/2 g piece of Si single crystal and Ge single crystal was used to calibrate the mass density of alcohol. Use of glass samples of 100 mg in size permitted mass density results in the set-up to yield an accuracy of 1% or less.

Molar volumes of the dry $(AgPO_3)_{1-x}(AgI)_x$ glass sample of set A and set B are summarized in figure 1. Also shown in figure 1 are molar volumes of glass samples reported by Sidebottom [26] and several crystalline standards including dry c-$AgPO_3$, α-AgI and β-AgI [38]. The value of V_M for c-$AgPO_3$ reported in figure 1 comes from a sample synthesized by crystallizing a $AgPO_3$ glass sample set A.

The present data on $V_M(x)$ show that the molar volume of the base glass, $AgPO_3$, is quite sensitive to water content, with wet samples having a lower molar volume than dry ones. For our dry $AgPO_3$ glass sample (set A) we found a mass density of 4.22 g cm^{-3}, or a molar volume of 44.24 cm^3. For our crystalline $AgPO_3$ sample, we found a mass density to be 4.24(43) g cm^{-3}, which translates into a molar volume of 44.05 cm^3. An earlier structure study [39] of c-$AgPO_3$ reported a mass density of 4.65 g cm^{-3}, which yields a molar volume of 40.18 cm^3, somewhat smaller than the value for our sample. Helical chains of PO_4 tetrahedra, in the presence of bonded water, compact as bridging O atoms are replaced by terminal OH$^-$ dangling ends. The splicing of chains must reduce the van der Waals-mediated interchain repulsion, and the mechanism could be operative in both the crystalline and glassy phases. Once water is bonded, terminal P–OH$^-$ bonds are formed and these are quite stable. The molar volumes of $(AgPO_3)_{1-x}(AgI)_x$ glass samples steadily decrease with increasing x, but the starting value of V_M at $x = 0$, controls in a significant way network packing as AgI is steadily alloyed in the base material as illustrated by the plots in figure 1.

2.3. X-ray diffraction

A crystalline $AgPO_3$ sample synthesized in the present work was characterized using a Rigaku Dmax-2100 x-ray diffractometer. The instrument uses a Cu target (Cu Kα radiation wavelength of 1.5406 Å). The diffraction data appear in figure 2. It reveals the characteristic reflections expected of the polymeric form of crystalline $AgPO_3$. The most intense Bragg peak in XRD results of our sample occurs at $2\Theta = 29.30$ and is found to be shifted to a lower value than the published result ($2\Theta = 31.67$) from the Joint Committee on Powder Diffraction Standards (JCPDS) data file #11-0640 [40]. We are in the process of performing a Rietveld analysis of our XRD data to reliably ascertain lattice parameters of our crystalline $AgPO_3$ sample, before comparing it to the published report [40].

2.4. Modulated-DSC

A model 2920 m-DSC from TA Instruments was used to study glass transitions. We used a $3\,°C\,min^{-1}$ scan rate and $1\,°C/100\,s$ modulation rate consistently throughout all measurements. Typically, about 15–20 mg of a sample in a platelet form was hermetically sealed in Al pans and placed in the head of the calorimeter along with a reference pan. Further details on the method can be found in the earlier reports [6, 34, 37]. The component of the total heat flow (figure 3 (green/grey)) that tracks the modulations is called the *reversing* (figure 3 (blue/black)) heat flow. The difference signal between the total and reversing heat flow signals represents the *non-reversing heat flow* signal [41] and it usually displays a Gaussian-like peak (figure 3 (red/light grey)) as a precursor to the glass transition [41]. The integrated area under the Gaussian profile gives the non-reversing enthalpy (ΔH_{nr}) at T_g. The frequency corrected ΔH_{nr} term was deduced in the usual way by subtracting the ΔH_{nr} term coming down in temperature from the corresponding term going up in temperature [34]. The frequency corrected ΔH_{nr} term is then independent of the modulated frequency [41]. The T_g value given by MDSC was deduced from the inflection point of the reversing heat flow step [41]. The quoted value of T_g of a sample is taken as the *mean value* of T_g (up) and T_g (down) of the reversing heat flow signal, i.e. $T_g = 1/2(T_g$ (up) $+ T_g$ (down)). Because of the finite scan rate of $3\,°C\,min^{-1}$ used in MDSC scans, there is a small but finite kinetic shift in T_g between T_g (up) and T_g (down) typically of about $2\,°C$ in our samples. By averaging, the deduced T_g represents a *scan-rate-independent* T_g. In each instance at least two samples at a given composition were studied from each batch preparation to check for reproducibility of results and ensuring homogeneity of samples.

MDSC scans were performed both on 'as-quenched or virgin' and 'T_g-cycled' glass samples [34]. The nature of the m-DSC scans on both 'as-quenched or virgin' and 'T_g-cycled' $AgPO_3$ base glass samples have been discussed elsewhere [34]. Representative m-DSC scans of present glasses (sample A) at $x = 5\%$ (stressed-rigid), 17% (intermediate) and 40% (flexible) recorded in the present work are given in figure 3. We find that the non-reversing enthalpy at the $x = 5\%$ (stressed-rigid) sample displays a broad peak (FWHM, $W = 35(2)\,°C$) that is asymmetric (high-T tail) and possesses a frequency-corrected integrated area, $\Delta H_{nr} = 368.4(5)$ mcal g^{-1}. At $x = 17\%$, a composition in the intermediate phase, the width $W = 25(2)\,°C$, $\Delta H_{nr} = 90.6(5)$ mcal g^{-1} and the peak becomes symmetric. At $x = 50\%$, a composition in the flexible phase, the width W decreases to $15(2)\,°C$, $\Delta H_{nr} = 276.3(5)$ mcal g^{-1} and the peak remains symmetric. These trends in the width W and shape of the non-reversing heat flow observed in the present glasses are quite similar to those seen earlier in covalent glasses [42] and serve to provide independent confirmation of the assigned elastic phases. We shall return to discuss these results in section 2.5.

A summary of the present m-DSC results appears in figure 4. In panel (a), we summarize the variation in $T_g(x)$ for both set of samples A and B. In general we find T_gs for both sets of samples to steadily decrease as the AgI content of
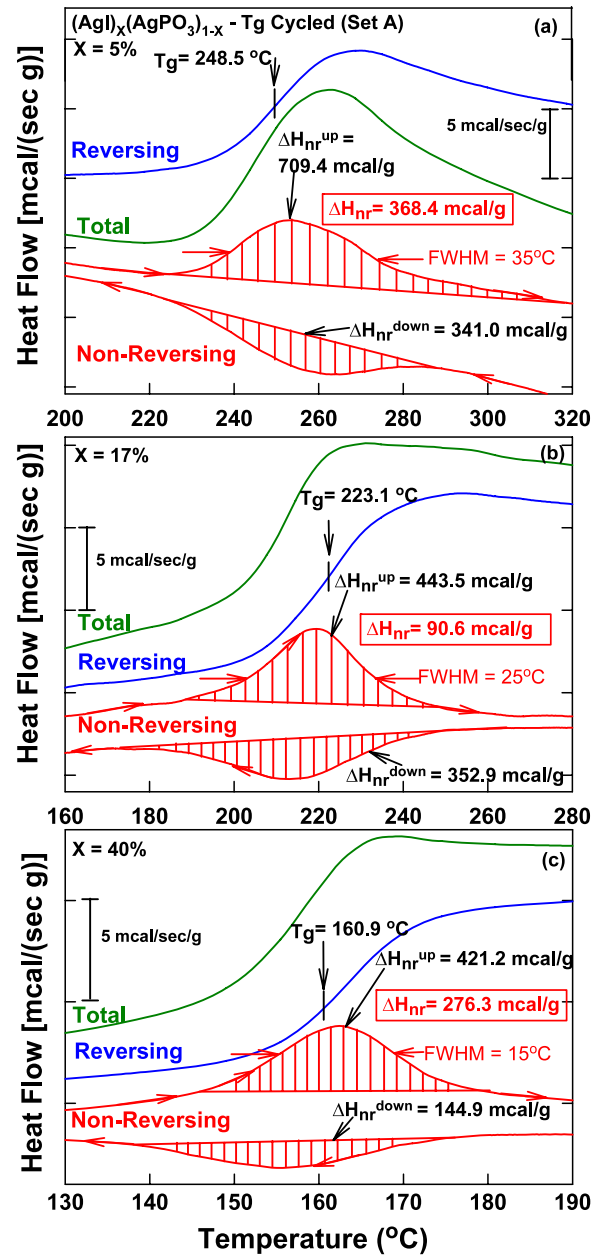

Figure 3. MDSC scans of present $(AgI)_x(AgPO_3)_{1-x}$ glasses (set A) at (a) $x = 5\%$ (stressed-rigid), (b) $x = 17\%$ (intermediate) and (c) $x = 40\%$ (flexible). Note that non-reversing enthalpy at the $x = 5\%$ sample displays a broad peak (FWHM, $W = 35(2)\,°C$) that is asymmetric (high-T tail). At $x = 17\%$ the width $W = 25(2)\,°C$ and the peak becomes symmetric. At $x = 50\%$ the width W decreases to $15(2)\,°C$ and the peak remains symmetric. These trends in the width W and shape of the non-reversing heat flow observed in the present glasses are quite similar to those seen earlier in covalent glasses.

the glasses increase. For samples of set B, T_gs are somewhat lower than in set A largely because these samples contain more water (see section 2.1). The present data are compared to two previous reports, one by Mangion–Johari [24] and a second one by Sidebottom [26], who used traditional DSC to establish T_g of their samples. In a traditional DSC experiment, T_g accessed from the inflection point of the (total) heat flow at a scan rate of
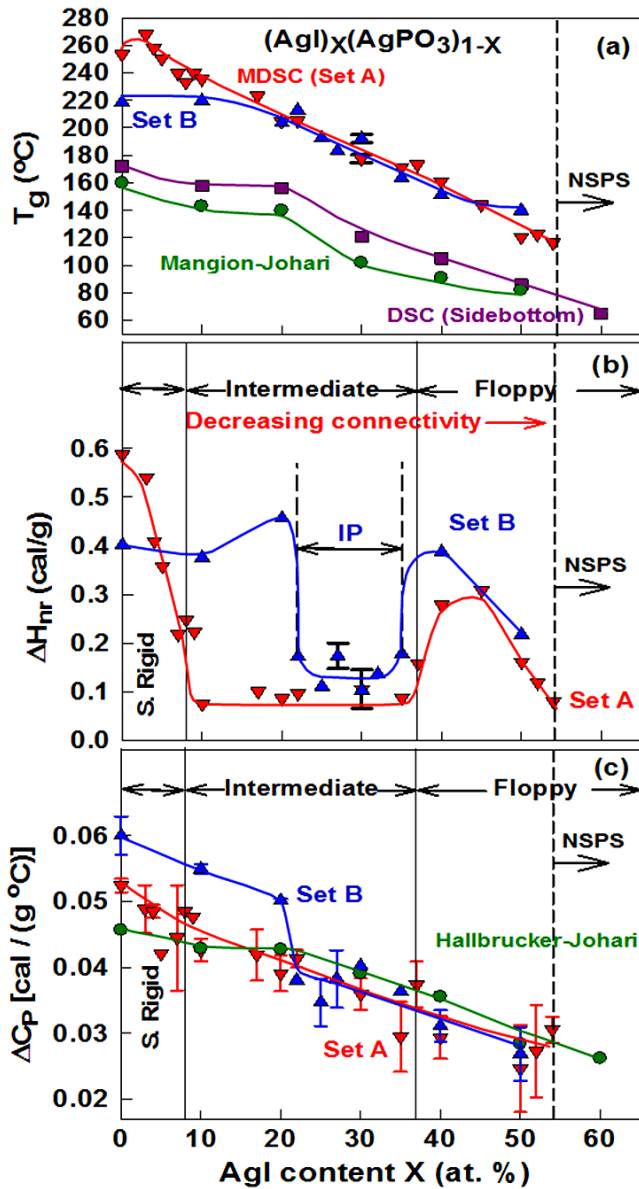
Figure 4. Variations in (a) $T_g(x)$, (b) non-reversing enthalpy $\Delta H_{nr}(x)$, and (c) heat capacity change at T_g, $\Delta C_p(x)$, in set A dry (▼), set B wet (▲) $(AgI)_x(AgPO_3)_{1-x}$ glass samples from present work. Also included for comparison are results reported by Mangion–Johari [24] (●), Sidebottom [26] (■) and Hallbrucker–Johari [22] (●). Note that presence of water in glass samples reduces T_g of the base material $(AgPO_3)$ and also the width of the reversibility window (compare set A with set B).

$20\,°C\,min^{-1}$ ($10\,°C\,min^{-1}$), would be kinetically shifted up by $8\,°C$ ($2\,°C$) in relation to m-DSC quoted T_g from our work. These technique-derived corrections to T_gs were established by performing DSC measurements on our samples. These corrections are small in relation to the observed differences in T_gs (ranging from 70 to $35\,°C$) between the present work and earlier [24, 26] work, and if applied would further increase the differences in T_g typically anywhere from 2 to $8\,°C$. These corrections are *not* reflected in the plot of figure 4. In these earlier reports, T_gs are also found to steadily decrease as x increases, although the starting value of T_g of the base material

$(AgPO_3)$ is significantly lower (by nearly $70\,°C$) than the value of the present samples, a reflection of their higher water content as discussed earlier [34].

In figure 4(b), we plot the observed variation in the non-reversing enthalpy, $\Delta H_{nr}(x)$, for both sets of samples, A and B. These data show that the $\Delta H_{nr}(x)$ term for the set of samples A shows a square-well-like global minimum in the $9\% < x < 38\%$ range [1], the reversibility window. In samples of set B, the reversibility window is found to be narrower, extending to the $20\% < x < 34\%$ range, and to be somewhat shallower in relation to the window in samples A. It is clear that the higher content of water present in samples of set B has a bearing on the reduced width of the reversibility window. Finally, in figure 4(c), we plot the variation in heat capacity change at T_g, $\Delta C_p(x)$ for samples in sets A and B, along with results reported earlier by Hallbruker and Johari [22] on the same glass system. The latter results have come from DSC measurements where one observes only the total heat flow in the scanning calorimetric measurements. It is interesting to note that the variation in $\Delta C_p(x)$ for the three different sets of samples show a steady decrease with increasing AgI content. We will comment on these data later.

2.5. Raman scattering

A model T64000 triple monochrometer Raman dispersive system from Horiba Jobin Yvon Inc, equipped with a CCD camera and a microscope (Olympus BX 41 with 80× objective) was used to study Raman scattering of the samples. The scattering was excited with 514.5 nm radiation with the laser beam focused to a 2 μm spot size (diameter) using typically 1.2 mW of power illuminating a sample. Measurements were performed at room temperature with the sample mounted in an MMR Joule–Thompson refrigerator [34] cold stage. Observed lineshapes were analyzed in terms of superposition of a suitable number of Gaussians to extract mode frequency, mode width and mode scattering strength intensity. Raman scattering is a powerful light scattering technique used to elucidate molecular structure of glass samples as will be illustrated here.

Figures 5 and 6 give a summary of Raman data on glass samples of set A in the low (0–440 cm^{-1}) and high (400–1400 cm^{-1}) frequency ranges. In the very low frequency range ($<50\ cm^{-1}$) (figure 5), we observe a broad mode usually identified as the boson mode, whose scattering strength intensity steadily increases as a function of the AgI content of glasses. At $x > 37.8\%$, this particular mode becomes the most intense feature of the observed lineshape in glasses. These features of our data are generally similar to those reported earlier by Fontana *et al* [43]. In our experiments, we have normalized Raman spectra at different compositions to the *same* laser power and, as a check of this normalization, we find mode scattering strength intensities in the bond-stretching regime to change systematically with x. Raman scattering is, in general, given as [44–46]

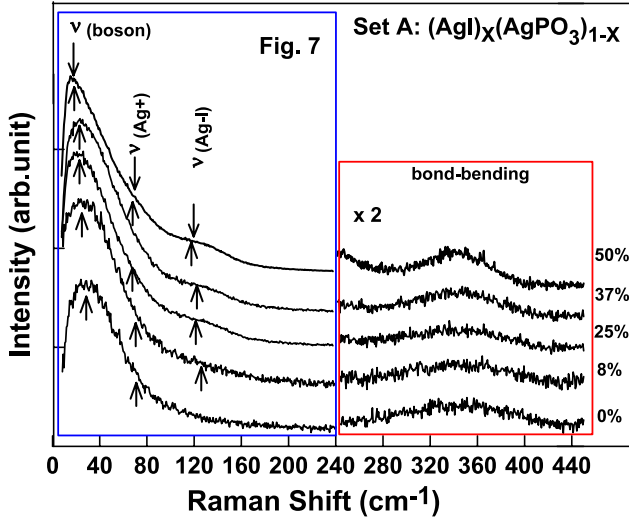$$I_{exp} = \frac{C(\omega)g(\omega)[n_B + 1]}{\omega}. \qquad (2)$$

Figure 5. Raman scattering on $(AgI)_x(AgPO_3)_{1-x}$ glass samples A in the low (0–400 cm^{-1}) frequency range. The observed lineshapes are analyzed in terms of three modes: a mode centered near 40 cm^{-1} (boson mode), a Ag$^+$ restrahlen mode near 85 cm^{-1} and a mode of AgI near 130 cm^{-1}. Scattering strength of these modes increases with AgI content (figure 7).

Figure 6. Raman lineshapes of present $(AgPO_3)_{1-x}(AgI)_x$ glass samples A at several different compositions. Broadly, these results suggest glass structure to transform from chain-like to ring-like as the AgI content increases.

In equation (2), $C(\omega)$ represents the photon–vibration coupling constant [47], $g(\omega)$ the vibrational density of states (VDOS) and n_B is the Bose occupation number. To analyze the low frequency (<200 cm^{-1}) modes in glasses, we obtained the reduced Raman scattering (I_{red}) from I_{exp}:

$$I_{red} = \frac{I_{exp}}{n_B + 1} \propto \frac{C(\omega)g(\omega)}{\omega} \qquad (3)$$

by dividing I_{exp} by the factor ($n_B + 1$). Since $C(\omega)$ varies [48] as $\sim\omega$ at frequencies $\omega > 20$ cm^{-1}, the ratio $\frac{I_{exp}}{n_B+1}$ provides a reasonable measure of the vibrational density of states $g(\omega)$. Reduced Raman scattering at selected glass compositions appear in figure 7. The effect of correcting for the finite T by obtaining I_{red} now yields lineshapes that show the low frequency modes to display symmetric peak-like features. The low frequency modes were analyzed in terms of three modes, one centered near 40 cm^{-1} (related to boson mode), a Ag$^+$ restrahlen mode near 85 cm^{-1} and a mode of AgI near 130 cm^{-1} (figure 7) [49–51]. Variations in the frequency and scattering strength reduced Raman intensity of the boson mode reveal thresholds near the stress ($x_c(1) = 9.5\%$) and rigidity ($x = x_c(2) = 37.8\%$) transition (figure 8), the two elastic thresholds observed in these glasses. The boson mode scattering strength intensity (figure 8(b)) shows a small step-like increase near $x_c(1)$ and a rather striking linear increase at $x > x_c(2)$. A linear extrapolation of the $I_{red}(x)$ data from $x = 37.8\%$ to 100% yields $I_{red}(x = 100) = 380$ counts and permits us to define a normalized scattering strength $I_{red}(x)/I_{red}(100)$ and a slope d$[I_{red}(x)/I_{red}(100)]/dx$. The linear behavior is characterized by a slope of 1.49 and we shall return to discuss these data in section 4.5.

At a slightly higher frequency (figures 5 and 6), we then observe *bond-stretching modes* associated with different
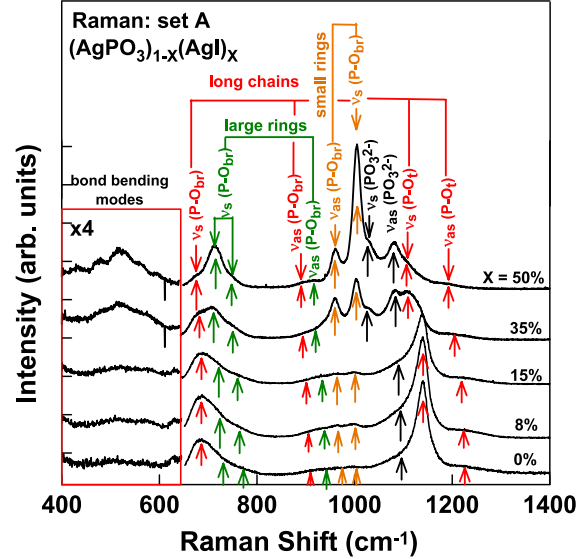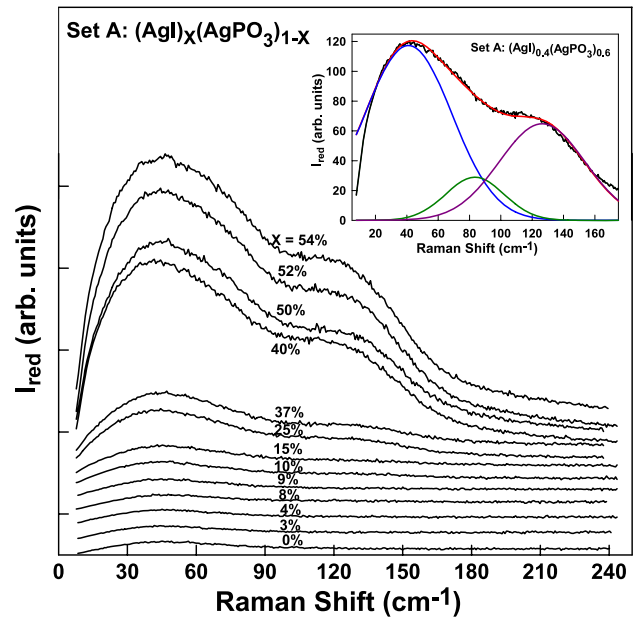

Figure 7. Reduced Raman scattering, $I_{red} = \frac{I_{exp}}{n_B+1} \propto \frac{C(\omega)g(\omega)}{\omega}$ of $(AgI)_x(AgPO_3)_{1-x}$ glass samples A at different glass compositions in the low (<200 cm^{-1}) frequency range. I_{exp} represent the experimental Raman scattering intensity, $C(\omega)$ the photon–vibration coupling constant [47], $g(\omega)$ the vibrational density of states (VDOS) and n_B the Bose occupation number. The inset shows the deconvolution of reduced Raman spectra of $(AgI)_x(AgPO_3)_{1-x}$ at $x = 40\%$ in terms of three modes as mentioned earlier in figure 5.

structural units [49–51] (300–650 cm^{-1} range). In the high frequency region (figure 6), we then observe *bond-stretching modes* of PO$_4$ units present in *chains* that steadily redshift and decrease in strength, as modes of PO$_4$ units in *small rings* and *large rings* steadily increase in scattering strength with
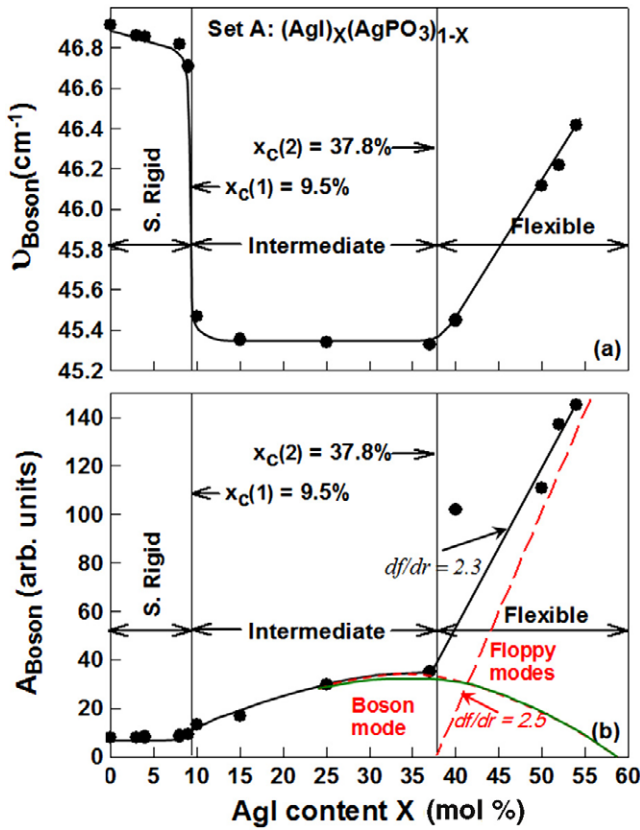
Figure 8. Variations in (a) the frequency and (b) scattering strength of the boson mode of $(AgI)_x(AgPO_3)_{1-x}$ glass samples A as a function of AgI content. Note that the results reveal thresholds near the stress ($x_c(1) = 9.5\%$) and rigidity ($x = x_c(2) = 37.8\%$) phase boundaries.

Figure 9. Infrared absorption of $(AgPO_3)_{1-x}(AgI)_x$ glass samples A at several indicated compositions.

increasing x. We shall return to discuss the mode assignments after presenting the IR reflectance data.

How do the present Raman data compare to previous results in the field?

Raman scattering in $(AgPO_3)_{1-x}(AgI)_x$ glass samples of set B (less dry) excited with 514.5 nm radiation show strong fluorescence compared to set A and the lineshapes did not change much with glass composition. Similar results were obtained by Shastry and Rao [52] at glass compositions of $x = 0.3, 0.4$ and 0.5, with T_gs respectively of 109, 95 and 87 °C. These T_gs are similar to those reported by Mangion and Johari [23] (figure 4(a)). Using 488 nm excitation, Shastry and Rao [52] were able to suppress fluorescence and obtained good Raman signals but their data also show little change in lineshape with AgI content. These differences of Raman lineshapes between the present results and earlier reports suggest that the molecular structure and thus the vibrational density of states of driest (high-T_g) and less dry (low-T_g) samples are quite different. We will return to discuss these data in section 4.

2.6. Infrared reflectance

Fourier transform infrared (FTIR) spectra were collected at room temperature using a Thermo Nicolet Nexus 870 FTIR bench. Specular reflectance measurements were made using a
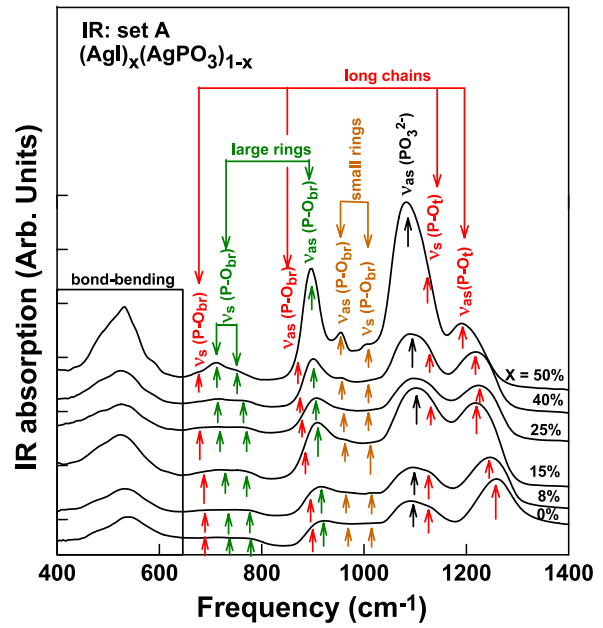
Seagull accessory, and a high reflectivity low carbon stainless steel mirror was used as reference to normalize the reflectivity signal. Each spectrum was collected for 200 scans at 8 cm^{-1} resolution. A proper combination of source, beamsplitters and detectors allowed collecting spectra in the 50–4000 cm^{-1} range. To obtain signals characteristic of our glass samples, we chose a reasonable thickness of the bulk samples with flat areas and gave no surface treatment prior to recording infrared reflectance. In these specular reflectance measurements the reflectance signal comes from the sample surface. Surface treatment such as polishing was therefore avoided so as not to change the surface structure of glasses [53]. Reflectivity data was then analyzed by Kramers–Kronig analysis to extract absorption signals. Figure 9 shows absorption signals at selected glass compositions (the same ones for which Raman data are presented in figure 6). These absorption signals were then least-squares fitted to a superposition of Gaussian profiles to extract mode frequency, intensity and width.

How do the infrared absorption data change as a function of AgI content? A number of observations can be made. First, a perusal of figure 9 shows that the asymmetric P–O$_t$ vibration mode in long chains systematically redshifts with AgI concentration. These IR results complement the Raman results of a redshift of the symmetric P–O$_t$ mode of long chains seen earlier in figure 6. Second, the intensity of the asymmetric mode of terminal PO$_3^{2-}$ groups is found to increase as the AgI content of the glasses increases (figure 9). The behavior is reminiscent of the corresponding symmetric vibrations in the Raman results (figure 6). Third, IR active modes characteristic of rings (970 and 900 cm^{-1}) grow at the expense of those of long chains (1300 cm^{-1}) as AgI content increases. Raman-active modes of rings (near 1000 and 700 cm^{-1}) grow at the expense of modes of long chains (near 1100 and 680 cm^{-1}). These observations taken together reveal that glass structure is

Table 1. AgPO$_3$ mode assignments.

Mode assignment	Present work Raman (cm^{-1})	Present work infrared (cm^{-1})	References
Boson	28.8	—	[43]
Ag$^+$ ion oscillations inside their oxygen cage	85	51.1 139.7	[38, 50]
ν_s (Ag–I)	130–120	130–120	[38, 50, 52]
Bond-bending modes of different structural units	650–300	650–300	• Kamitsos *et al* [50] and Velli *et al* [49] suggested that mode at 650–400 cm^{-1} is composed of bending modes of different structural units. • Nelson and Exarhos [51] suggested that mode at 360–300 cm^{-1} is composed of pendent and in-chain P–O$_t$ bending modes
ν_s (P–O$_{br}$) long chain	686.6	685.9	[52, 60, 50]
ν_s (P–O$_{br}$) large ring	766.3 and 733.7	773 and 731	[60]
ν_{as} (P–O$_{br}$) long chain	900	894	[60, 50]
ν_{as} (P–O$_{br}$) large ring	920.3	917.3	[60, 50]
ν_{as} (P–O$_{br}$) small ring	971	969.4	[60, 50]
ν_s (P–O$_{br}$) small ring	1008	1010.5	[60, 50]
ν_{as} (PO$_3^{2-}$)	1087	1103.8	[50, 49]
ν_s (PO$_3^{2-}$)	1029	—	[60]
ν_s (P–O$_t$) long chain	1140	1162.5	[52, 60, 50]
ν_{as} (P–O$_t$) long chain	1235.5	1256.2	[60, 50]

steadily getting less connected as AgI is introduced into the base AgPO$_3$. Wakamura *et al* [54] and Bhattacharya *et al* [55] have also reported on IR results on this glass system, and our results differ from these earlier reports. These differences come from the sample make-up and also in the way these samples were measured. In their experiments, Bhattacharya *et al* [55] performed transmission measured using platelets of intimately mixed finely powdered glass samples with CsI, an IR transmitting matrix.

2.7. Raman and infrared vibrational mode assignments

The complementary role of Raman scattering and Infrared reflectance serves as a powerful diagnostic tool for mode assignments. In general, for a centrosymmetric molecule such as PO$_4$ tetrahedral units, no Raman-active vibration is also infrared-active and no infrared-active vibration is also Raman-active. The exclusion rule [56] is quite useful in mode assignments. In the present case PO$_4$ tetrahedra do not have a center of inversion and, as a result, the two modes of the tetrahedral molecule are both Raman-and IR-active (asymmetric stretching and bending) and two other modes are only Raman-active (symmetric stretching and bending). We shall see that symmetric vibrational modes are strongly excited in Raman scattering but weakly in IR reflectance: on the other hand, asymmetric modes are strongly excited in IR reflectance but weakly in Raman scattering. The power of IR reflectance as a probe of both *free* water [57, 58] and bonded water as the OH stretch vibrations of P–OH$^-$ bonds [57, 59] has been widely recognized. In a previous contribution we illustrated the idea for the case of the base AgPO$_3$ glass [34].

Mode assignments. In comparing the Raman and IR reflectance data on AgI–AgPO$_3$ glasses (figures 6 and 9) the complementary nature of activity of certain vibrational modes becomes apparent. These features of the present data along with previous work in the field, has permitted making mode assignments. P–O$_t$ *modes.* The highest frequency modes (1235 and 1140 cm^{-1}) observed can be identified respectively with the asymmetric and symmetric modes of P–O$_t$ bonds of PO$_4$ tetrahedra. The asymmetric mode (1235 cm^{-1}) is strongly excited in IR but weakly in Raman scattering. The reverse is the case for the symmetric vibration, as expected. *Defect* (PO$_3$)$^{2-}$. The next two lower frequency modes, one near 1087 cm^{-1} and the other near 1029 cm^{-1}, represent respectively the asymmetric and symmetric vibrations of a (PO$_3$)$^{2-}$ unit that forms part of a pyrophosphate grouping of Ag$_2$P$_2$O$_7$ units [49, 50, 60]. In this dimeric unit, two PO$_4$ tetrahedra share a bridging oxygen and the mode in question represents the P–O$_t$ vibrations of these pair of Q^1 species (in NMR notation). The asymmetric (1087 cm^{-1}) mode of PO$_3^{2-}$ units is strongly excited in IR but weakly in Raman scattering. On the other hand, the reverse is the case for the symmetric mode (1029 cm^{-1}) of these units (table 1). Our data shows that the concentration of these dimeric units steadily increases as AgI content of glasses increases (figure 9). *Long chain* P–O$_{br}$ *modes.* We identify the modes near 686 and 900 cm^{-1}, respectively, with the symmetric and asymmetric vibrations P–O$_{br}$ bonds present in long chains (table 1) of PO$_4$ units. The symmetric vibration is strongly excited in Raman scattering (figure 6) but weakly in IR. The reverse circumstance prevails for the asymmetric stretch of the P–O$_{br}$ bonds in long chains. The higher vibrational mode frequencies of P–O$_t$ modes in

relation to P–O$_{br}$ ones are consistent with the smaller P–O$_t$ bond length (145 pm) than P–O$_b$ bond lengths (160 pm) [61]. *Large ring modes.* As long chains transform into large rings and smaller rings, one expects the vibrational mode frequency of the P–O$_{br}$ bonds to up-shift in frequency as a lowering of the P–O$_{br}$–P bridging oxygen bond angle [60] must occur to require closure of small rings. We identify the modes near 750 and near 920 cm^{-1} with the symmetric and asymmetric vibrations of large rings. The feature near 750 cm^{-1} is actually split into two modes, 733 and 766 cm^{-1}, and we note that both these modes are strongly excited in Raman while their asymmetric counterparts are strongly excited in IR (figure 9). *Small ring modes.* The complementary activity of the two vibrational modes near 970 and 1000 cm^{-1} in Raman and IR responses suggests that these modes are the asymmetric and symmetric vibrations of small rings. In table 1 we have summarized the present assignments along with suitable references to previous work in the field that broadly support our findings.

2.8. Raman optical elastic power laws

The narrow vibrational mode associated with symmetric stretch of P–O$_t$ bonds in Raman scattering of sample set A (figure 6) is reasonably well resolved. This particular mode is of interest because it describes the vibrational motion of *all* PO$_4$ tetrahedra in the structure of the glasses. These tetrahedra are cross-linked across Ag$^+$ cations and are vibrationally coupled. With increasing AgI content, the mode softens and tracks the elastic softening of the backbone. A parallel behavior of a softening of the P–O$_t$ mode in Raman scattering of the present glass system was also observed by Fontana *et al* [43]. With fewer compositions studied over the glass forming range, for these authors, it was apparently not possible to recognize evidence of two thresholds, one near 15% and the other near 40% of AgI (figure 2 of [43]) present in their data. We have analyzed the redshift of the mode quantitatively by least-squares fitting the observed lineshapes to extract the width, frequency and integrated intensity of the modes in question. Figures 10(a) and (b) give a summary of the results on the variation of the P–O$_t$ symmetric mode frequency in Raman experiments, and separately the P–O$_t$ asymmetric mode frequency in IR absorption experiments as a function of AgI. We observe the P–O$_t$ symmetric mode to systematically redshift as the AgI content of the glasses increases.

In both Raman and IR responses, we find that the observed variation in mode frequencies displays *two* vibrational thresholds [1], one near $x = 9.5\%$ and the other near $x = 37.8\%$. These thresholds coincide with the walls of the reversibility window (figure 4(b)). The frequency variation of the symmetric P–O$_t$ mode observed in Raman scattering can be analyzed further to extract underlying optical elastic power laws in the intermediate phase and in the stressed-rigid phase as we illustrate next.

In figure 10(a), the curvature in the $\upsilon(x)$ plot of the symmetric stretch mode frequency of P–O$_t$ bonds in the stressed-rigid and in the intermediate phase can be analyzed by fitting the observed mode frequency squared $\upsilon^2(x)$ to the
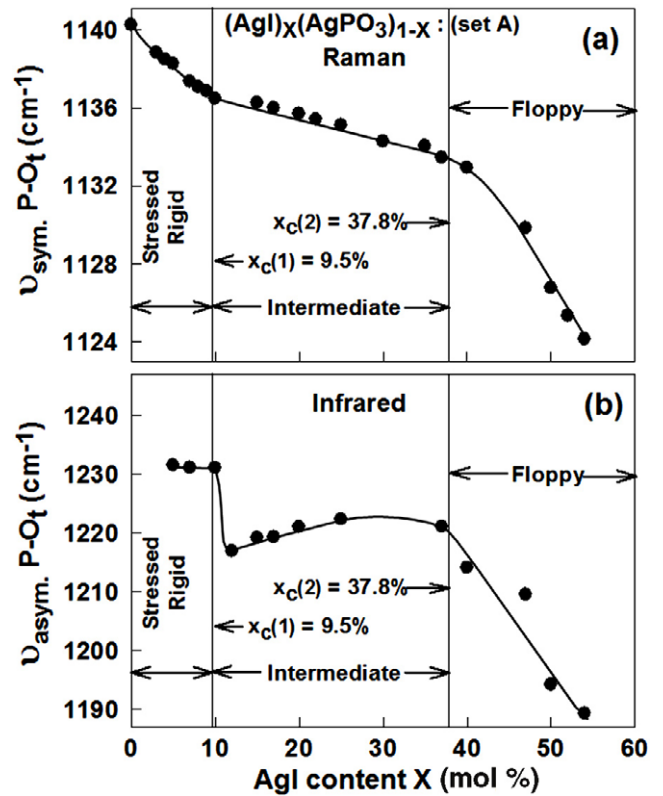

Figure 10. Variations in (a) the P–O$_t$ symmetric mode frequency in Raman scattering and (b) the P–O$_t$ asymmetric mode frequency in infrared absorption experiments as a function of AgI. Note that the P–O$_t$ symmetric and asymmetric modes systematically redshift with increasing x to display two thresholds, one near $x_c(1) = 9.5\%$ and a second near $x_c(2) = 37.8\%$.

following equation:

$$\upsilon^2(x) - \upsilon_c^2(1) = A[x - x_c(1)]^{p_1} \qquad (4)$$

where $\upsilon_c(1)$ represents the threshold value of $\upsilon(x)$ at $x = x_c(1) = 9.5\%$, the stress transition [1], and p_1 the elastic power law. The optical elastic power law in the stressed-rigid phase, $p_1 = 1.25(2)$, is thus determined from the slope of a log–log plot shown in figure 11(a) A similar procedure was used to extract the elastic power law in the intermediate phase as illustrated in figure 11(b), and a power law, $p_2 = 0.98(3)$ is obtained using the rigidity phase boundary $x_c(2) = 37.8\%$. We shall return to discuss these results in section 2.9.

2.9. AC electrical conductivity

Glass sample discs about 10 mm in diameter and 2 mm thick were synthesized by pouring melts into special troughs. Platelets were then thermally relaxed by cycling through T_g. Platelets then were polished and the Pt electrodes deposited. Platelets were spring loaded into a sample holder and AC conductivity measurements were taken using an Impedance spectrometer (Solartron SI 1260) as a function of temperature in the 200 K $< T < T_g$ range, and as a function of frequency in the 1 Hz $< f < 10^6$ Hz range. The room temperature conductivities for each glass samples were

Figure 12. Variations in electrical conductivity $\sigma(x)$ ($\blacktriangledown$) and activation energy for conductivity $E_A(x)$ ($\bullet$) of the present $(AgPO_3)_{1-x}(AgI)_x$ glass samples A with glass composition. The frequency dependence of conductivity permits fixing the high frequency permittivity and the Coulomb energy E_C ($\blacklozenge$). The resulting variations in the strain energy ($\blacktriangle$) $E_S = E_A - E_C$ shows the term to remain high in the stressed-rigid phase but to decrease in the flexible phase.
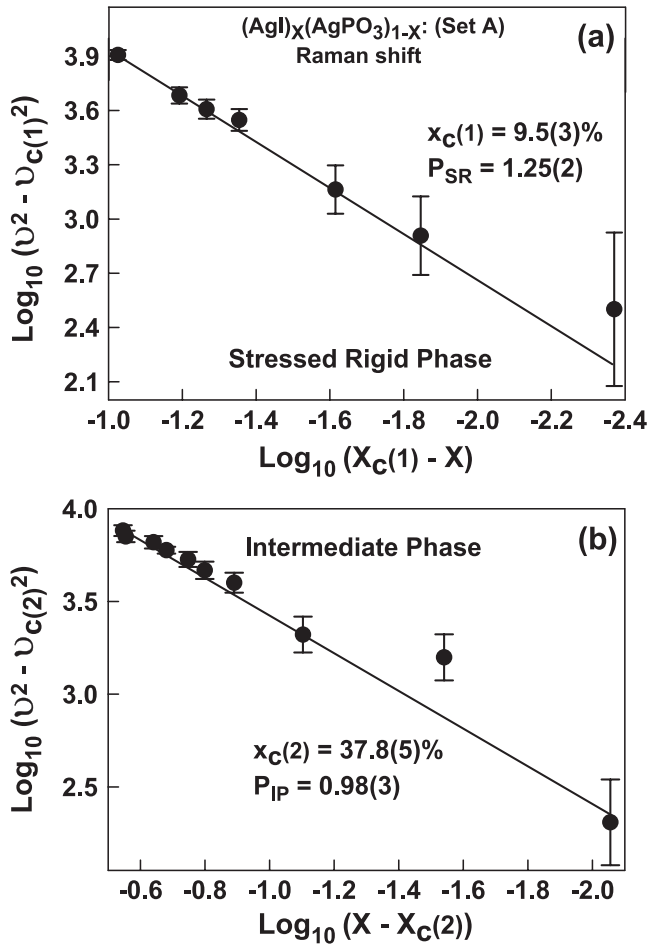

Figure 11. (a) shows a plot of $\log_{10}(\nu^2 - \nu_c(1)^2)$ against $\log_{10}(x_c(1) - x)$ in the $0 < x < 9.5\%$ range and gives the optical elastic power law in the stressed-rigid glass samples A, $p_1 = 1.25(2)$. (b) shows a plot of $\log_{10}(\nu^2 - \nu_c(2)^2)$ against $\log_{10}(x_c(2) - x)$ in the $9.5\% < x < 37.8\%$ range and gives the optical elastic power law in the intermediate phase of glass samples A, $p_2 = 0.98(3)$.

deduced from AC electrical conductivity measurements at low frequencies when f approaches 0. The activation energies (E_A) for electrical conductivity for all of the glass samples were extracted from the Arrhenius plot of the dc electrical conductivity as a function of temperature. Further details on the AC electrical conductivity measurement used in the present work is described elsewhere [1]. The Coulomb energy (E_C) for ion creation was estimated in the usual way [1] and the resulting strain energy $E_S = E_A - E_C$ was then obtained. Figure 12 shows a plot of the compositional trends in conductivity $\sigma(x)$ along with $E_A(x)$, $E_C(x)$ and $E_S(x)$ data on the present electrolyte glasses.

How do the present results on $\sigma(x)$ compare with earlier ones on the present electrolyte glasses? In figure 13(b) we show compositional trends in $\sigma(x)$ from several earlier studies including those of Bhattacharya *et al* [55], Sidebottom [26], Mangion and Johari [24] and Malugani *et al* [62], along with the present findings in figure 13(a). The $\sigma(x)$ results of Malugani *et al* [62] and Sidebottom [26] agree with each other over a wide range of compositions. On the other hand, the $\sigma(x)$ data of Bhattacharya *et al* [55] are nearly two orders
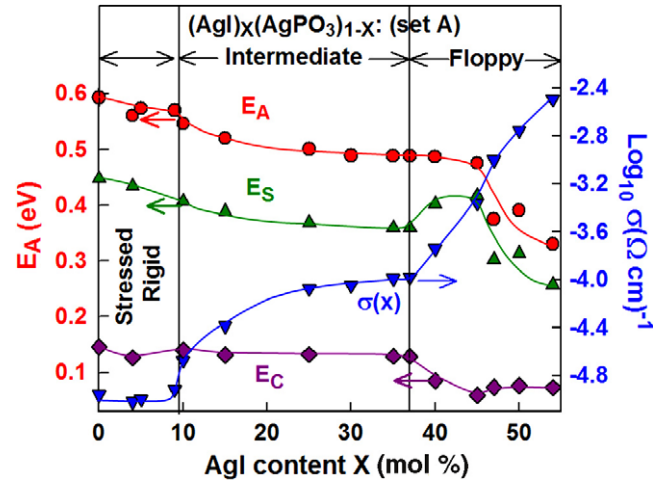
Figure 13. Variations in room temperature conductivities, $\sigma(x)$, in (a) present glass samples A ($\blacktriangledown$), and (b) those reported by Mangion–Johari [23, 24] ($\bullet$ and $\star$), Sidebottom [26] ($\blacksquare$), Bhattacharya *et al* [55] ($\blacklozenge$) and Malugani *et al* [62] ($+$).

of magnitude higher than those of Malugani *et al* [62]. The $\sigma(x)$ data of Mangion and Johari [24] are quite similar to those of Malugani *et al* [62] at $x > 40\%$, but at lower x their data lie in between those of Bhattacharya *et al* [55] and

Sidebottom [26]. These earlier data are in sharp contrast to the variation of $\sigma(x)$ reported by us which displays two distinct thresholds. The conductivity of the base AgPO$_3$ glass ($x = 0$), reported by various groups differ substantially from each other (figure 13(b)) and we have suggested that variability of these data is due to the presence of water impurities [34] Once water is incorporated in the base material, it transforms from being elastically stressed-rigid to flexible, and one no longer expects the conductivity to display the two thresholds, as will be discussed later.

3. Lagrangian constraints in AgPO$_3$ and AgI glass

AgI exists in an orthorhombic phase (β) at room temperature. At $T > 150\,°C$ it transforms to a cubic (α) solid electrolyte phase. In this phase Ag migrates across tetrahedral and trigonal interstitial sites resulting in high ionic conductivity ($10^{-1}\ \Omega^{-1}\ cm^{-1}$). In an earlier contribution [3], the Lagrangian constraints associated with the α phase were estimated assuming that only bond-stretching forces were intact for both Ag and I. Since Ag is mobile, the bond-bending forces centered on Ag and on I must be weak and thus assumed to be intrinsically broken. Such a model of the α phase is a good starting point to describe the glass, which would be the case only if the glass were a fast-ion conductor [3]. These estimates place the constraints/atom, $n_c = 2$, for AgI glass, suggesting a mean coordination number $r = 2$. AgI glass is thus expected to be an elastically flexible system. The glass transition temperature of AgI is also expected to be low ($\sim 50\,°C$) since $r = 2$, as is indeed observed when AgI is alloyed in base chalcogenide glasses [3] In this context, a model glass to compare AgI glass would be Se ($r = 2$) with a T_g of $40\,°C$.

Crystalline AgPO$_3$ is composed of PO$_4$ tetrahedra arranged in helical chains [39]. In a helical pitch there are 4 tetrahedral units. In each PO$_4$ tetrahedral unit, a phosphorus atom possesses a coordination number (r) of 4 with two bridging (O$_b$) and two terminal (O$_t$) oxygen atoms. Ag sits between these chains in a distorted tetragonal pyramid having a nominal coordination number of 5. However, two of these 5 Ag–O bonds are short (~ 2.40 A) and the other three bonds are somewhat longer (~ 2.50 A) [39]. The two short Ag–O bonds are to terminal oxygen atoms in a chain, as one would have expected with Ag$^+$ compensating for the two terminal O$^-$ atoms. In the glassy phase, the simplest assumption is that the near-neighbor bonding constraints with the 2 O$_t$ are strong and intact while those with the 3 more distant bridging oxygen atoms are weaker and intrinsically broken. In this *limiting case*, the coordination numbers of P, O$_b$, O$_t$ and Ag become, respectively, 4, 2, 2 and 2. An atom with coordination $r(>2)$, has $r/2$ bond-stretching and $2r - 3$ bond-bending forces. The Lagrangian constraints for P, O$_b$, O$_t$ and Ag are then, respectively, 7, 2, 2 and 2. For an AgPO$_3$ formula unit ($N = 5$), we enumerate the Lagrangian constraints as

$$5n_c = \left[7(P) + \tfrac{1}{2} \times 2 \times 2(O_b) + 2 \times 2(O_t) + 2(Ag) \right] = 15 \tag{5a}$$

$$\text{or} \qquad n_c = 3. \tag{5b}$$

In the *limiting case*, the AgPO$_3$ glass is thus viewed as an example of an isostatically rigid network. In practice, this appears nearly to be the case. Our experiments show AgPO$_3$ glass to be a weakly *stressed-rigid* glass ($n_c > 3$), we suppose because the Ag residual constraints with the three more distant oxygen near-neighbors cannot be totally excluded. However, upon alloying a mere 9 mol% of AgI, interchain spacing increases enough to lift the residual constraints, and an isostatically rigid alloyed glass is realized at the onset of the reversibility window (figure 4(b)). The coordination number decrease of Ag with O is independently corroborated by coherent x-ray scattering results [63] on these glasses that show a decrease from 5.1 at $x = 0$ to 2.5 at $x = 0.5$.

In summary, these considerations on Lagrangian constraints suggest that AgPO$_3$ glass can be expected to be mildly stressed-rigid and AgI glass to be elastically flexible. In the present solid electrolyte glasses, AgPO$_3$–AgI, the underlying networks should steadily soften as the AgI content of these glasses is steadily increased.

4. Discussion

4.1. Molecular structure of glasses

AgPO$_3$ glass is widely regarded [35, 39, 61, 64] to be made up of polymeric chains of PO$_4$ tetrahedral units, and glass structure has often been compared to one of its crystalline [35, 39] polymorphs, which is made up of helical chains of PO$_4$ units. Raman scattering from AgPO$_3$ glass and its polymeric crystalline counterpart is dominated by two vibrational modes, one due to the symmetric stretch of P–O$_t$ bonds (1140 cm^{-1}) and the other due to symmetric stretch of P–O$_{br}$ bonds (686 cm^{-1}) [34, 49, 51, 52, 60, 61, 65–67]. In the crystalline phase these modes are rather narrow (linewidths ~ 6 cm^{-1}) but in the glass these modes are understandably broader (linewidth ~ 40 cm^{-1}) [34] due to intrinsic structural disorder. One also observes weaker features in Raman vibrational density of states of AgPO$_3$ glass that can be identified to the characteristic symmetric and asymmetric P–O$_{br}$ vibration of *large rings* near 766–733 and 920 cm^{-1} observed, respectively, in Raman and IR responses. The corresponding vibrational features of *small rings* include the symmetric and asymmetric stretch of P–O$_{br}$ bonds near 1000 cm^{-1} and 970 cm^{-1} observed, respectively, in Raman and IR responses (table 1, figures 6 and 9). This is not all that surprising given that crystalline AgPO$_3$ also exists in a tetrameric form composed of four-membered rings of PO$_4$ tetrahedra. In addition, one observes Raman vibrational density in the 300–650 cm^{-1} range that can be identified with the bending modes of different structural PO$_4$ units (table 1, figures 5 and 6).

Upon comparing Raman with the IR in glasses one finds that vibrational features attributed to large and small rings steadily increase in integrated intensity at the expense of those of polymeric chains. For example, in Raman scattering the symmetric stretch vibrations of P–O$_{br}$ bonds in small rings ~ 1000 cm^{-1} and large rings (~ 766–733 cm^{-1}) far exceed the integrated intensity of the corresponding vibration in long

chains (680 cm^{-1}) as $x \sim 50\%$. A similar pattern is noted in the IR absorption data shown in figure 9. One finds, for example, the asymmetric P–O$_{br}$ mode in large rings ~ 920 cm^{-1} and small rings near 970 cm^{-1} to systematically evolve in strength as the corresponding P–O$_{br}$ mode in long chains near 900 cm^{-1} steadily decreases as the AgI content of glasses increases to 50%. These results lead us to believe that, with increasing concentration of AgI, glass structure steadily evolves from polymeric chain-like at low x to becoming ring-like as x increases to 50%.

The structure of the present glasses has been examined in neutron diffraction [27] and x-ray diffraction experiments, which reveal a first sharp diffraction peak (FSDP) at anomalously low momentum transfer $Q \sim 0.7$–0.8 cm^{-1}. The FSDP is widely regarded as a signature of intermediate range order in glasses. Reverse Monte Carlo modeling of the neutron and x-ray structure factors by Wicks *et al* [27] and Borjesson *et al* [12] have suggested that the FSDP is related to the increased interchain spacing of polymeric phosphate chains as AgI is alloyed. The insertion of the AgI additive between polymeric chains drives them apart and shifts the FSDP to lower Q values in the experiments, as confirmed by the calculations. Alternative suggestions [28, 64, 68] of the FSDP in terms of segregation of AgI-rich clusters in the glasses are not only inconsistent with the x-ray and neutron structure factors, but also with the existence of a solitary glass transition that steadily decreases with AgI content (figure 4(a)).

The broad picture of structure described above appears to be supported by the present Raman results at low AgI additive, $x > 25\%$. In figures 6, the vibrational mode near 1140 cm^{-1}, ascribed to PO$_t$–Ag$^+$ chain segments, is found to steadily soften (figure 10(a)). We can understand a weakening of the intrachain P–O$_t$ bonding interactions at the expense of interchain PO$_t$–Ag$^+$ ones as more Ag$^+$ cations become available between the chains. However, as $x > 25\%$, a better description of the glasses consists of visualizing them to be made of large and small rings of PO$_4$ tetrahedra and fragmented Ag$_2$P$_2$O$_7$ pyrophosphate units rather than polymeric chains. This is not unexpected given that the base glass, AgPO$_3$, as noted earlier, is also known to exist in a crystalline polymorph that consists of tetramers. Rings pack better than chains and probably account for the decreasing molar volume (figure 1) as the AgI content of the glasses increase. The loss of global connectivity associated with the chain to ring transition of the network structure leads to two elastic phase transitions from mildly rigid to flexible glasses as x increases to 54%.

4.2. Three elastic phases in $(AgPO_3)_{1-x}(AgI)_x$ glasses

The central finding of the present work is the existence of three distinct elastic regimes in the present electrolyte glasses as their connectivity is lowered by alloying the electrolyte salt. Several pieces of experimental data bear on the subject including (i) the non-reversing enthalpy at T_g, (ii) Raman optical elastic power laws and (iii) the nature of the glass transition endotherms.

4.2.1. Non-reversing enthalpy at T_g.
The non-reversing enthalpy at T_g, $\Delta H_{nr}(x)$, displays a wide, deep and sharp

reversibility window in the present glasses (figure 4(b)). Such windows were observed earlier in covalent glasses [69] and were identified with networks that belong to a phase that is elastically rigid but unstressed, also known as the intermediate phase (IP). In analogy to those findings, we thus identify the compositional window, $9.5\% < x < 37.8\%$, (figure 4(b)) with the IP in the present electrolytes. In covalent glasses atoms usually bond in conformity to the $8 - N$ coordination rule facilitating estimates of network connectivity by a count of the mean coordination number r. It is usually defined as

$$r = \left(\frac{1}{N}\right) \Sigma n_i r_i \tag{6}$$

where $(\frac{n_i}{N})$ and r_i designate, respectively, the fraction of atoms i possessing a coordination number r_i. In the present electrolytes atom valences, and particularly that of the mobile Ag, are not satisfied locally [13] and estimates of network connectivity pose new challenges. However, we note that the connectivity of the end member glass compositions, namely AgPO$_3$ ($r > 2.4$) and AgI ($r = 2$) have been estimated using constraint counting algorithms (section 3), and these data unequivocally suggest that the mean coordination number r (or network connectivity) of the present glasses must steadily decrease as x increases. That view is independently corroborated by the measured glass transition temperatures $T_g(x)$, which steadily decrease as x increases (figure 4(a)). Stochastic agglomeration theory [70] has shown that T_g provides a reliable measure of network connectivity. These considerations suggest that glass compositions at low x, $0 < x < 9.5\%$, must belong to the *stressed-rigid phase*, those at high $x > 37.8\%$ to the flexible phase, while compositions at intermediate values of x ($9.5\% < x < 37.8\%$) to the Intermediate phase. These assignments are corroborated by Raman optical elastic power laws, as we discuss next.

4.2.2. Raman optical elastic power laws.
Raman scattering experiments in covalent systems have proved to be particularly diagnostic in identifying the different elastic regimes of network glasses through measurements of optical elastic power laws. The conditions that have made Raman scattering a rewarding probe of elastic phases in glasses were discussed in a recent review [36]. Numerical experiments on stochastic amorphous Si networks modeled by a Keating potential, i.e. bond-stretching and bond-bending forces, reveal elastic constants (C_{11}) to increase as a power law [71, 72] in the stressed-rigid regime:

$$C_{11} \approx (r - r_c)^p \tag{7}$$

with $p \sim 1.4$. In these simulations networks of different connectivity r are made by cutting bonds. Here r_c represents the phase boundary between flexible and stressed-rigid elastic phases.

In the Raman scattering experiments a selected vibrational mode is chosen and the square of the mode frequency (proportional to optical elasticity) is studied as a function of glass composition (network connectivity). The selected vibrational mode in question must belong to a local structure

that forms part of the connective tissue and is usually close to being optimally constrained. In the group IV chalcogenides, corner-sharing (Ge or Si) $(Se_{1/2})_4$ tetrahedra that are strongly Raman-active have been particularly useful probes [73, 74, 36] of elastic behavior in the chalcogenide glasses.

In the present electrolyte glasses the symmetric stretch of $P–O_t$ bonds in PO_4 tetrahedra give rise to a strongly excited Raman band near 1140 cm^{-1}. This band encompasses contributions from PO_4 tetrahedra present in long chains, large rings and small rings. In section 2.8, we have deduced from analysis of the Raman data the elastic power law in the stressed-rigid phase, $p_1 = 1.25(3)$, and in the intermediate phase, $p_2 = 0.98(3)$. These power laws, surprisingly, are found to be remarkably similar to the ones reported earlier in covalent systems. For example, in ternary $Ge_xP_xSe_{1-2x}$ glasses [36], the elastic power law in the stressed-rigid phase, $p_2 = 1.48(2)$, and in the intermediate phase, $p_1 = 0.98(1)$. Parallel results are found in other covalent systems [3, 73]. To summarize, the measured Raman elastic power laws in the present electrolyte glass strongly support the suggested identification of the three elastic phases from the non-reversing enthalpy at T_g.

4.2.3. Nature of glass transition endotherms.   In the chalcogenide glasses we have observed that the non-reversing heat flow in the three elastic phases displays characteristic trends. In the flexible phase, the heat flow term usually displays a narrow (~20 °C) and symmetric temperature profile, with the enthalpy slowly increasing as glasses age. In the intermediate phase the heat flow term displays a minuscule enthalpy that shows little or no ageing. In the stressed-rigid phase the non-reversing heat flow term is usually broad and displays an asymmetric temperature profile with the underlying enthalpy steadily increasing upon ageing of the glasses. These characteristics of the non-reversing heat flow in covalent systems have close parallels to those in the present electrolyte glasses (section 2.4). Although we have not investigated ageing effects in the present electrolytes, we observe the non-reversing heat flow endotherm to be wide and asymmetric at $x < 9.5\%$, and to be narrow and symmetric at $x > 37.8\%$, trends that follow the ones noted in chalcogenides earlier.

4.3. Role of water impurities on physical behavior of AgPO₃–AgI glasses

The samples investigated in the present work differ from the ones reported by earlier groups [24, 26, 55] by virtue of synthesis, and we believe our samples are dryer and contain less water. How does that influence the physical properties and structures of glasses? It may be useful to begin the discussion by reviewing results on the present samples, particularly comparing results on set A (driest) with set B (less dry). If one compares T_g and V_M data one finds a distinct pattern; T_gs of samples in set B are lower than those of set A by anywhere from about 40 to 10 °C (figure 4(a)) and molar volumes of samples in set B are lower than those of set A by anywhere from 4.5% to 0.5% (figure 1). Likewise, T_gs of samples reported by Sidebottom are 60 °C lower than those found in

samples of set A (figure 4(a)) while molar volumes (V_M) of his samples are anywhere from 4.76% ($x = 0$) to 11.8% ($x = 50\%$) lower that the ones observed by us for samples of set A. T_gs of samples reported by Mangion and Johari are anywhere from 100 to 60 °C lower than those of samples in set A. These data suggest that the presence of water in samples lowers T_g and molar volumes [59, 75], and the handling of precursors in a dry ambient is necessary to minimize water uptake by samples [34, 35].

The underlying structural issues bears on chains of $−P−O−P−$ steadily depolymerizing by the presence of water impurities for which evidence comes from IR absorption experiments that reveal features [34, 57] characteristic of P–OH$^-$ vibrations near 1637, 2318 and 2352 cm^{-1}. With increasing AgI content of the present glasses these vibrational features reduce in strength but never vanish even for the set of samples A. The presence of depolymerized chains lower the connectivity of the network, which is reflected in the T_gs of the samples. Depolymerized chains apparently pack better, which is clearly reflected in the molar volumes of glasses.

A significant finding of the present work is the strong (factor of 3 or more) enhancement of the mid-IR response of glasses with increasing AgI content, a feature that is readily seen in comparing the response at $x = 0$ with the one at $x = 50\%$, both in the bond-stretching and bond-bending regimes (figure 9). The observation is reminiscent of the mid-IR response enhancement (at least by a factor of 4) in wet AgPO₃ glasses in relation to dry ones [34] which was traced to collective modes of water locking on to the Ag$^+$ floppy modes and lead to a long range coherent enhancement of oscillator strength of all optical modes of chains. A similar circumstance, most likely, exists in the present dry glasses with AgI salt (playing the same role as that of water in) dressing the surfaces of the smaller structural motifs such as small rings and pyrophosphate groupings and transferring the collective modes of AgI salt by locking on to Ag$^+$ floppy modes and lead to long range coherent enhancement of optical modes.

The very striking role played by traces of water impurities in the narrowing of the reversibility window [37] in going from the set A to the set B samples is illustrated in figure 4(b). We find, for example, that $x_c(1)$ shifts up from 9.5% to 22%, while $x_c(2)$ shifts down from 37.8% to 35%, thus narrowing the intermediate phase width from $\Delta x = x_c(2) − x_c(1) = 28\%$ in set A to nearly 13% in set B samples. IR response of these glasses reveals largely bonded water with little or no evidence of free water in the samples. Replacement of bridging oxygen atoms in chains by dangling OH$^-$ ends serves to splice the P–O–P chain network and reduce the range of glass compositions across which a stress-free network can persist. These findings are reminiscent of the collapse of intermediate phases of chalcogenide glasses (GeSe₄ and GeS₄) when alloyed by iodine [76]. Halogen atoms in the chalcogenides serve to replace bridging chalcogen (S, or Se) atoms and disrupt the network structure by creating dangling Ge–I ends [76]. At present we are uncertain on aspects of local or intermediate range structures that control the width of the IP in the present electrolyte glasses, and this is a point of continuing investigations.

4.4. Ionic conductivity and network flexibility

The AC conductivity results on the present electrolyte glass system raise two obvious questions: how does one reconcile the two-step-like variation in $\sigma(x)$ observed here with earlier work in the field? Secondly, what is the microscopic origin of these two steps in $\sigma(x)$? We begin by addressing these issues. T_g endotherms of dry $AgPO_3$ glasses are characteristic of stressed-rigid networks [34], while those of wet samples are characteristic of flexible networks. Wet samples possess not only lower T_gs but also have a non-reversing heat flow term [34] that is narrow and symmetric in T, features that we have identified [42, 77] earlier with flexible glasses. Once the base glass has been rendered flexible by water doping one does not expect to observe the stress and rigidity transitions and their consequences on conductivity (see sections 2 and 4.3). Thus, the two thresholds observed in $\sigma(x)$ in the present work are characteristic of *dry* samples and represent the intrinsic behavior of the electrolyte glasses. These were not observed in earlier reports largely because samples reported upon in the literature, to the best of our knowledge, are wet samples in which the base oxide ($AgPO_3$) is already flexible.

The small increase in conductivity near $x \sim 9.5\%$ can be traced to the small decrease in strain activation energy ΔE_s (figure 12) as glasses become stress-free at $x > 9.5\%$. In this range of compositions, we visualize glass structure to be largely composed of polymeric PO_4 chains (figures 6 and 9) that become separated as AgI is inserted between them. Such a simple structural description was, in fact, proposed many years ago by Wicks *et al* [27], as mentioned earlier. These hard-sphere Monte Carlo simulations also showed evidence of Ag^+ diffusivities increasing precipitously at $x > 25\%$. This composition is not that far from the composition, $x_c(1) = 9.5\%$, observed in our experiments. We attribute the increase in conductivity of glasses at $x > 9.5\%$ to result from the weakly alloyed chain glass structure becoming stress-free.

The real structure of these electrolyte glasses, especially at higher AgI concentrations, is likely to be different than the one described by the reverse Monte Carlo simulations [12, 27]. The present Raman and IR data reveal that there exists a transition from a chain-like to a ring-like structure as the AgI content $x > 40\%$ and glasses soften and become elastically flexible at $x > x_c(2) = 37.8\%$. The exponential increase of conductivity in the flexible phase give rises to a power law [1], $\mu = 1.78(10)$ (figure 14). This value is in excellent agreement with the predicted power law ($\mu = 2.0$) of conductivity percolation in 3D resistor networks [78]. These data suggest that there must exist in the electrolyte glasses percolation paths for Ag^+ ions to hop along. At low x these paths must be isolated or decoupled. But as the concentration of these paths increases with x, these paths must percolate and contribute to the logarithmic increase of conductivity once $x > 37.8\%$. To gain better insights into these conductivity thresholds more sophisticated structural models of these glasses have to be constructed that can at least predict the intermediate phase reported here. It would then, realistically, be possible to model the second conductivity transition near $x = x_c(2)$. A power-law variation of conductivity with alkali modifier concentration in borate glasses has been modeled using Monte
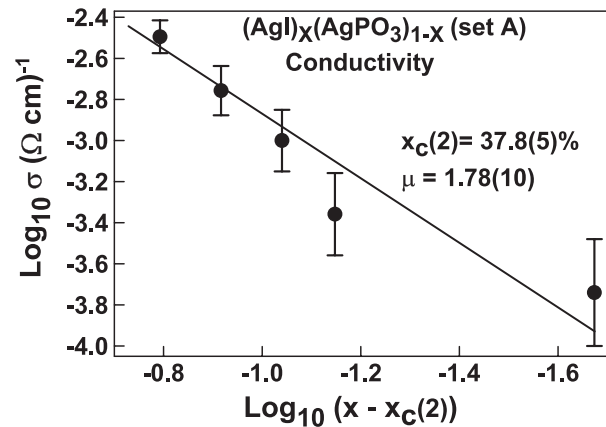

Figure 14. A plot of $\log_{10} \sigma$ against $\log_{10}(x - x_c(2))$ yielding conductivity power law, $\mu = 1.78(10)$ in the flexible phase, with $x_c(2) = 37.8\%$ in the present glass samples A.

Carlo simulations by Maass *et al* [79] assuming ions to take on characteristic local environments, and it remains to be seen if there are any commonalities with the present approach.

Experimental evidence for the filamentary nature of ionic conduction in the present electrolyte glasses at $x = 50\%$ (flexible phase) have come from field-ion microscopy measurements of Escher *et al* [80]. These authors examined emission from tips of wires made of $(AgI)_{50}(AgPO_3)_{50}$. In their experiments they imaged tips as a function of time and observed several bright spots identified with Ag^+ ion emission centers. These centers are thought to arise from nanometer-sized ion channels terminating on tips. These field-ion measurements confirm in a direct way the conductivity enhancement predicted by the 3D percolation behavior in the present electrolyte glasses.

The broader issue raised by the present results bears on the fundamental interactions that determine fast-ion transport and network structural interactions in glasses: are they quite as different as generally believed in the field, or are they the same as recently suggested by Ingram *et al* [18]? The large decoupling index R_τ observed in glasses generally result because *activated volumes* for ion transport are much smaller than for structural relaxation. The elastic interactions that are active in ion hopping at short and long timescales, and that locally deform a network to create a doorway for an ion to hop across, are essentially the same in nature that lead to mechanical relaxation of the network as a whole. In our experiments, the AgI salt provides carriers to the base $AgPO_3$ glass and it also elastically softens the matrix. As long as the matrix is stiff carriers are localized: however, as the matrix softens ion transport becomes pervasive.

Evidence for channel or filamentary conduction is also found in metal-modified silicates. The findings in the silicates have a strong bearing on the behavior observed in the present electrolyte system. In silicates, it has been found both from molecular dynamics simulations [81, 82] and experiments [83, 84] that a new intermediate range order emerges with the addition of alkali network modifiers. In silica-rich compositions, local intra-channel hopping prevails,

leading to high activation barriers and low ionic conductivities. However, with increasing alkali content evidence of clustering is suggested, and at $x > 16\%$ these clusters join to create channels in a modified random network. New characteristic metal–metal distances appear as manifested in, for example, pair correlation functions. The composition at which such micro-segregation sets in turns out to be the elastic phase boundary between stressed-rigid and intermediate phases [85]. In silicates, percolation of channels and the onset of conduction are clearly related to the intermediate phase.

The present electrolyte glass system, much like the silver iodomolybdates, are examples of strongly decoupled systems, yet one finds that in both these systems conductivity is largely controlled by the elasticity of the network. The case of molten salts such as $2Ca(NO_3)_2 \cdot 3KNO_3$ or CKN is of interest because these are examples of mildly decoupled electrolytes. In these systems, modeling studies show [86] that the frequency dependence of σ can be related to the dynamical properties of melts, again supporting the view that basic interactions that control ion transport, and separately network structure relaxation, are essentially the same. The equivalence of the Ngai coupling model [83, 87, 88] with Funke's concept of mismatch generated relaxation for the accommodation and transport of *ion*s [87] (migration) reinforces the view that compliance of the disordered matrix plays a central role in determining ion transport in electrolyte glasses.

4.5. Boson and floppy modes in elastically flexible phase

Presence of excess vibrations over Debye-like ones (density of states $g(\omega) \sim \omega^2$) due to a redistribution of the vibrational density of states in glasses over their crystalline counterparts usually gives rise to a feature in the low frequency range (10–50 cm^{-1}) called the boson mode. These excess modes have been observed in Raman scattering [89] and in inelastic neutron scattering. The origin of these low frequency vibrations in a disordered solid has been the subject of ongoing discussions [89–91]. One view is to regard glasses to be heterogeneous, i.e. to possess a domain structure. Strong intra-domain forces lead atoms to vibrate coherently in a domain. Weak inter-domain forces lead to soft modes associated with transverse acoustic vibrations usually attributed to the boson mode [89].

Flexible networks are characterized by floppy modes while stressed-rigid ones by the absence of such modes. Consider, for example, the case of an Se glass composed of a 3D network of polymeric chains. In a chain each Se atom has two near-neighbors, $r = 2$, and this leads to one bond-stretching ($r/2 = 1$) and one bond-bending ($2r - 3 = 1$) constraint, for a total of two Lagrangian constraints/Se atom (n_c) [92, 93]. Ideas on constraints were first introduced [93] by Lagrange to facilitate solving problems in classical mechanics nearly two centuries ago. Here the Se chain network is composed of covalent bonds regarded as Hookian springs. And since there are three degrees of freedom (n_d) per Se atom, one finds that there are not enough bonding constraints to exhaust the available degrees of freedom. The flexibility of an Se chain glass derives from this deficit, or the presence of one floppy mode/atom which represents the difference

$n_d - n_c = 1$. Floppy modes also represent the number of zero-frequency solutions of the secular determinant [92] in vibrational analysis, and in practice these are shifted to finite frequencies due to residual interactions [93]. They are observed in Lamb–Mossbauer factors [94] and in inelastic neutron scattering experiments [95, 96]. In rigidity theory flexibility of networks is mathematically cast in terms of the count of floppy modes per atom f as discussed by Thorpe [92]. And as an Se chain network is steadily cross-linked by alloying, for example, a group IV element like Ge, the mean coordination number r increases and the count of floppy modes/atom decreases (equation (8)). In such a mean-field counting of constraints, generally ascribed to the work of Phillips [93], a network becomes elastically stressed-rigid, when $f(r)$ vanishes as r increases to 2.40:

$$f = 6 - \left(\frac{5}{2}\right)r. \tag{8}$$

Note that the magnitude of the slope $|\mathrm{d}f/\mathrm{d}r| = 2.50$ in such a mean-field approach to percolation of rigidity.

Do floppy modes have a bearing to boson modes in glasses? The observation of the three elastic phases and the availability of rather complete compositional trends in frequency and scattering strength of the boson mode (figure 8) offer the opportunity to address the basic issue. As mentioned earlier, variations in the boson mode frequency and scattering strength display two thresholds that coincide with the two elastic thresholds, unequivocally showing the elastic behavior of these glasses must have a direct bearing on boson modes. The linear increase in the Bose mode scattering strength $\mathrm{d}[I_{\mathrm{red}}(x)/I_{\mathrm{red}}(100)]/\mathrm{d}x = 1.41$ at $x > 37.8\%$ (figure 8) invites the following comment. In 3D networks, rigidity theory has shown [96] that the count of floppy modes per atom (f) decreases linearly with mean coordination number r, with a slope $\mathrm{d}f_{\mathrm{theo}}/\mathrm{d}r = 2.50$. In the present electrolyte glasses, the connection between glass composition x and its mean coordination number r is not as obvious as in covalent networks, largely because the valence of ions is usually not satisfied locally. We had recognized several years ago [3] that the end member composition, $x = 100\%$, of AgI glass is topologically equivalent to a chain of atoms in which each atom has two neighbors, i.e. $r = 2$, such as in glassy Se. We now make the simplest assumption [92] that the mean coordination number r at the onset of rigidity in the present electrolytes (at $x = 37.8\%$) has a value of 2.40. The assumption permits us to directly connect changes in x to those in r. Secondly, we assume that the observed normalized scattering strength, $I_{\mathrm{red}}(x)/I_{\mathrm{red}}(100)$ is a measure of the floppy mode count variation with r, and $f = 1$ at $x = 100\%$ when $r = 2$. Under these two assumptions, one can show that the observed slope $\mathrm{d}[I_{\mathrm{red}}(x)/I_{\mathrm{red}}(100)]/\mathrm{d}x = 1.41$ translates to a $|\frac{\mathrm{d}f_{\mathrm{obs}}(x)}{\mathrm{d}r}|$ of 2.30(3), which may be compared to the rigidity theory predicted slope $|\frac{\mathrm{d}f_{\mathrm{theo}}(x)}{\mathrm{d}r}|$ of 2.50. These data strongly suggest that the observed boson mode in the flexible phase (at $x > 37.8\%$) of the present glasses represents floppy mode excitations. The most natural interpretation of the present data can be schematically illustrated by the plot shown in figure 8(b). In the flexible glasses, floppy modes largely

contribute to the boson mode, as shown by the broken line with a slope $|\frac{\mathrm{d}f_{\mathrm{theo}}(x)}{\mathrm{d}r}| = 2.50$. And as glasses enter the intermediate phase at $x < 37.8\%$, soft modes contribute to the boson mode. This particular feature of a growth in the soft mode scattering in the intermediate phase is not well understood at present, but we note that earlier results on Ge_xSe_{1-x} glasses are consistent with that finding [45].

The identification of floppy modes contributing to low frequency modes in Raman scattering of the present electrolyte glass system is profound for another reason. To date floppy modes have been identified in Se_n chain bearing covalent networks as arising from the lack of dihedral angle restoring forces [97]. In the present electrolyte glasses, there are no twofold coordinated chains, but the system configurationally evolves in an identical fashion. For an AgI glass, there is one floppy mode per atom that contributes to its flexibility. The microscopic origin of this mode is at present not entirely obvious.

In summary, the present findings on low frequency vibrations observed in Raman scattering on a prototypical solid electrolyte glass show that the so-called boson mode has contributions from both soft modes and floppy modes, with the former contributing in the mildly rigid elastic phase and the latter in the flexible elastic phase. Ideas on elastic behavior of glasses, commonplace in covalent solids, apparently also extend to ionic solids including fast-ion conducting system.

5. Conclusions

In the present work we have demonstrated the existence of three distinct regimes of elastic behavior in dry $(AgI)_x(AgPO_3)_{1-x}$ glasses, $0\% < x < 9.5\%$ stressed-rigid, $9.5\% < x < 37.8\%$. Intermediate, $x > 37.8\%$ flexible. Raman optical elasticity power laws, trends in the nature of the glass transition endotherm corroborate the three elastic phase assignments. Ionic conductivity measurements reveal a step-like increase when glasses become stress-free at $x > x_c(1) = 9.5\%$ and a logarithmic increase in conductivity once glasses become flexible at $x > x_c(2) = 37.8\%$ in the dry samples with a power law $\mu = 1.75$. The power law is suggestive that the logarithmic increase results due to percolation of 3D filamentary conduction pathways. These data represent the intrinsic behavior of dry glasses, which are in contrast to earlier reports on wet glasses synthesized by handling precursors in laboratory ambient environment, which reveal a monotonic increase in conductivity with the solid electrolyte fraction but no steps. These data demonstrate rather directly the central role of network flexibility in controlling ion transport in a prototypical decoupled glass.

The widely different relaxation times for ion transport and structural relaxation in glasses derives from the underlying size of volumes impacted by these processes, which is minuscule (less than 1 A^3) in the former and global ($\sim cm^3$) in the latter. However, in both these cases process compliance or elasticity has the same magnitude as illustrated by the unified approach of Ingram *et al* [18]. These ideas bring glasses and polymer electrolytes on the same platform, and are in harmony with the present finding that elastic flexibility of solid electrolyte backbones promotes ion transport.

Variations of boson mode frequency and scattering strength display two thresholds that coincide with the two elastic phase boundaries. In the flexible phase, scattering strength of the boson mode increases almost linearly with glass composition x, with a slope that tracks the *floppy mode fraction* as a function of mean coordination number r predicted by mean-field rigidity theory. These data unequivocally show that the excess low frequency vibrations contributing to boson mode in flexible glasses must come in large part from *floppy modes*.

Acknowledgments

Note added in proof. We would like to draw attention to the work of Naumis that bears on floppy modes and Lamb–Mossbauer factors [98]. On a separate note, an analysis of the AC conductivity results including the Coulomb energy (E) from a Modulus analysis has permitted a more reliable estimate of the Strain energy (E_S) in $AgPO_3$–AgI glasses. Implications of these findings on AC conductivity, and particularly the three compositional regimes has been examined by Malki *et al* [99].

References

[1] Novita D I, Boolchand P, Malki M and Micoulaut M 2007 *Phys. Rev. Lett.* **98** 195501
[2] Saienga J and Martin S W 2008 *J. Non-Cryst. Solids* **354** 1475
[3] Boolchand P and Bresser W J 2001 *Nature* **410** 1070
[4] Minami K, Mizuno F, Hayashi A and Tatsumisago M 2007 *Solid State Ion.* **178** 837
[5] Mitkova M and Kozicki M N 2007 *J. Phys. Chem. Solids* **68** 866
[6] Holbrook C, Chen P, Novita D I and Boolchand P 2007 *IEEE Trans. Nanotechnol.* **6** 530
[7] Angell C A 1992 *Annu. Rev. Phys. Chem.* **43** 693
[8] Ingram M D 1987 *Phys. Chem. Glasses* **28** 215
[9] Howell F S, Bose R A, Macedo P B and Moynihan C T 1974 *J. Phys. Chem.* **78** 639
[10] Adams S and Swenson J 2000 *Phys. Rev. Lett.* **84** 4144
[11] Roling B 2001 *Phys. Chem. Chem. Phys.* **3** 5093
[12] Borjesson L, McGreevy R L and Howells W S 1992 *Phil. Mag.* B **65** 261
[13] Swenson J and Adams S 2001 *Phys. Rev.* B **64** 024204
[14] Elliott S R 1994 *Solid State Ion.* **70** 27
[15] Angell C A 1986 *Solid State Ion.* **18/19** 72
[16] Greaves G N and Ngai K L 1994 *J. Non-Cryst. Solids* **172** 1378
[17] Torell L M and Angell C A 1988 *Br. Polym. J.* **20** 173
[18] Ingram M D, Imrie C T, Ledru J and Hutchinson J M 2008 *J. Phys. Chem.* B **112** 859
[19] Pappin A J, Ingram M D, Hutchinson J M, Chryssikos G D and Kamitsos E I 1995 *Phys. Chem. Glasses* **36** 164
[20] Ingram M D, Hutchinson J M and Pappin A J 1991 *Phys. Chem. Glasses* **32** 121
[21] Oyama Y and Kawamura J 1992 *Solid State Ion.* **53–56** 1221
[22] Hallbrucker A and Johari G P 1989 *Phys. Chem. Glasses* **30** 211
[23] Mangion M and Johari G P 1987 *Phys. Rev.* B **36** 8845
[24] Mangion M and Johari G P 1988 *Phys. Chem. Glasses* **29** 225
[25] Kartini E, Collins M F, Priyanto T, Yusuf M, Indayaningsih N, Svensson E C and Kennedy S J 2000 *Phys. Rev.* B **61** 1036
[26] Sidebottom D L 2000 *Phys. Rev.* B **61** 14507
[27] Wicks J D, Borjesson L, Bushnellwye G, Howells W S and McGreevy R L 1995 *Phys. Rev. Lett.* **74** 726

[28] Tachez M, Mercier R, Malugani J P and Dianoux A J 1986 *Solid State Ion.* **20** 93

[29] Rousselot C, Malugani J P, Mercier R, Tachez M, Chieux P, Pappin A J and Ingram M D 1995 *Solid State Ion.* **78** 211

[30] Benassi P, Fontana A and Rodrigues P A M 1991 *Phys. Rev.* B **43** 1756

[31] Minami T 1985 *J. Non-Cryst. Solids* **73** 273

[32] Ravaine D 1985 *J. Non-Cryst. Solids* **73** 287

[33] Swenson J and Borjesson L 1996 *Phys. Rev. Lett.* **77** 3569

[34] Novita D I and Boolchand P 2007 *Phys. Rev.* B **76** 184205

[35] Mustarelli P, Tomasi C, Magistris A and Scotti S 1993 *J. Non-Cryst. Solids* **163** 97

[36] Boolchand P, Jin M, Novita D I and Chakravarty S 2007 *J. Raman Spectrosc.* **38** 660

[37] Rompicharla K, Novita D I, Chen P, Boolchand P, Micoulaut M and Huff W 2008 *J. Phys.: Condens. Matter* **20** 202101

[38] Mercier R, Tachez M, Malugani J P and Rousselot C 1989 *Mater. Chem. Phys.* **23** 13

[39] Jost V K H 1961 *Acta Crystallogr.* **14** 779

[40] Research Department, R& E Division, Monsanto Chemical Company Dayton-Ohio, USA personal communication

[41] Thomas L C 2007 *Modulated DSC Technology* T.A. Instruments, Inc. chapter 5 (Delaware: Measurement of Glass Transitions and Enthalpic Recovery) p 43 (http//www.TAInstruments.com)

[42] Boolchand P, Georgiev D G and Micoulaut M 2002 *J. Optoelectron. Adv. Mater.* **4** 823

[43] Fontana A, Rossi F, Armellini C, D'Angelo G, Tripodo G and Bartolotta A 1999 *Phil. Mag.* B **79** 2073

[44] Yannopoulos S N, Andrikopoulos K S and Ruocco G 2006 *J. Non-Cryst. Solids* **352** 4541

[45] Boukenter A and Duval E 1998 *Phil. Mag.* B **77** 557

[46] Duval E, Garcia N, Boukenter A and Serughetti J 1993 *J. Chem. Phys.* **99** 2040

[47] Shuker R and Gammon R W 1970 *Phys. Rev. Lett.* **25** 222

[48] Duval E, Boukenter A and Achibat T 1990 *J. Phys.: Condens. Matter* **2** 10227

[49] Velli L L, Varsamis C P E, Kamitsos E I, Moncke D and Ehrt D 2005 *Phys. Chem. Glasses* **46** 178

[50] Kamitsos E I, Kapoutsis J A, Chryssikos G D, Hutchinson J M, Pappin A J, Ingram M D and Duffy J A 1995 *Phys. Chem. Glasses* **36** 141

[51] Nelson B N and Exarhos G J 1979 *J. Chem. Phys.* **71** 2739

[52] Shastry M C R and Rao K J 1990 *Spectrochim. Acta* A **46** 1581

[53] Baidullaeva A, Vlasenko A I and Mozol P E 1997 *Semiconductors* **31** 1234

[54] Wakamura K, Katagi J and Takahashi H 1999 *Physica* B **263** 799

[55] Bhattacharya S, Dutta D and Ghosh A 2006 *Phys. Rev.* B **73** 104201

[56] Cotton F A 1990 *Chemical Applications of Group Theory* (New York: Wiley–Interscience)

[57] Efimov A M and Pogareva V G 2000 *J. Non-Cryst. Solids* **275** 189

[58] Colthup N B, Daly L H and Wiberley S E 1990 *Introduction to Infrared and Raman Spectroscopy* (San Diego, CA: Harcourt Brace)

[59] Naraev V N 2004 *Glass Phys. Chem.* **30** 367

[60] Rulmont A, Cahay R, Liegeois-Duyckaerts M and Tarte P 1991 *Eur. J. Solid State Inorg. Chem.* **28** 207

[61] Brow R K 2000 *J. Non-Cryst. Solids* **263** 1

[62] Malugani J P, Wasniewski A, Doreau M, Robert G and Al Rikabi A 1978 *Mater. Res. Bull.* **13** 427

[63] Takahashi H, Matsubara E and Waseda Y 1994 *J. Mater. Sci.* **29** 2536

[64] Tachez M, Mercier R, Malugani J P and Chieux P 1987 *Solid State Ion.* **25** 263

[65] Rossi F, Fontana A and Righetti L 2002 *Phil. Mag.* B **82** 323

[66] Bobovich Y S 1962 *Opt. Spektrosk. [Opt. Spectrosc. (USSR)]* **13** 492

[67] Matic A, Boerjesson L, Wannberg A and McGreevy R L 1996 *Solid State Ion. Diffus. React.* **86–88** 421

[68] Rousselot C, Tachez M, Malugani J P, Mercier R and Chieux P 1991 *Solid State Ion.* **44** 151

[69] Selvanathan D, Bresser W J, Boolchand P and Goodman B 1999 *Solid State Commun.* **111** 619

[70] Micoulaut M 2007 *J. Optoelectron. Adv. Mater.* **9** 3235

[71] He H and Thorpe M F 1985 *Phys. Rev. Lett.* **54** 2107

[72] Franzblau D S and Tersoff J 1992 *Phys. Rev. Lett.* **68** 2172

[73] Selvanathan D, Bresser W J and Boolchand P 2000 *Phys. Rev.* B **61** 15061

[74] Qu T, Georgiev D G, Boolchand P and Micoulaut M 2003 The intermediate phase in ternary $Ge_xAs_xSe_{1-2x}$ glasses *Supercooled Liquids, Glass Transition and Bulk Metallic Glasses* vol 754, ed T Egami, A L Greer, A Inoue and S Ranganathan (Warrendale, PA: Materials Research Society) p 157

[75] Richet P 2005 *Phys. Chem. Glasses* **46** 333

[76] Wang F, Boolchand P, Jackson K A and Micoulaut M 2007 *J. Phys.: Condens. Matter* **19** 226201

[77] Boolchand P, Micoulaut M and Chen P 2008 Nature of glasses *Phase Change Materials: Science and Applications* ed S Raoux and M Wuttig (Heidelberg: Springer) p 37

[78] Zallen R 1983 *The Physics of Amorphous Solids* (New York: Wiley)

[79] Maass P, Bunde A and Ingram M D 1992 *Phys. Rev. Lett.* **68** 3064

[80] Escher C, Latychevskaia T, Fink H W and Pohl D W 2006 *Phys. Rev. Lett.* **97**

[81] Huang C D and Cormack A N 1990 *J. Chem. Phys.* **93** 8180

[82] Vessal B, Greaves G N, Marten P T, Chadwick A V, Mole R and Houdewalter S 1992 *Nature* **356** 504

[83] Greaves G N and Ngai K L 1995 *Phys. Rev.* B **52** 6358

[84] Greaves G N 1985 *J. Non-Cryst. Solids* **71** 203

[85] Vaills Y, Qu T, Micoulaut M, Chaimbault F and Boolchand P 2005 *J. Phys.: Condens. Matter* **17** 4889

[86] Singh P, Banhatti R D and Funke K 2005 *Phys. Chem. Glasses* **46** 241

[87] Funke K and Banhatti R D 2007 *J. Non-Cryst. Solids* **353** 3845

[88] Ngai K L and Capaccioli S 2007 *J. Phys.: Condens. Matter* **19** 205114

[89] Duval E, Mermet A and Saviot L 2007 *Phys. Rev.* B **75** 024201

[90] Leonforte F, Tanguy A, Wittmer J P and Barrat J L 2006 *Phys. Rev. Lett.* **97** 055501

[91] Taraskin S N, Loh Y L, Natarajan G and Elliott S R 2001 *Phys. Rev. Lett.* **86** 1255

[92] Thorpe M F and Chubynsky M V 2001 The intermediate phase and self-organization in network glasses *Phase Transitions and Self-Organization in Electronic and Molecular Networks* ed J C Phillips and M F Thorpe (New York: Kluwer Academic/Plenum) p 43

[93] Boolchand P, Lucovsky G, Phillips J C and Thorpe M F 2005 *Phil. Mag.* **85** 3823

[94] Boolchand P, Enzweiler R N, Cappelletti R L, Kamitakahara W A, Cai Y and Thorpe M F 1990 *Solid State Ion.* **39** 81

[95] Kamitakahara W A, Cappelletti R L, Boolchand P, Halfpap B, Gompf F, Neumann D A and Mutka H 1991 *Phys. Rev.* B **44** 94

[96] Phillips W A, Buchenau U, Nücker N, Dianoux A J and Petry W 1989 *Phys. Rev. Lett.* **63** 2381

[97] Wang Y, Nakaoka T and Murase K 2001 Thermal relaxation and criticality of the stiffness transition *Phase Transitions and Self-Organization in Electronic and Molecular Networks* ed J C Phillips and M F Thorpe (New York: Kluwer Academic/Plenum) p 85

[98] Naumis G 2006 *Phys. Rev.* B **73** 172202

[99] Malki M, Micoulaut M, Novita D, Goodman B and Boolchand P 2009 Rigidity and flexibility of glassy networks and fast-ion conduction *Rigidity and Boolchand Intermediate Phases in Nanomaterials* ed M Popescu and M Micoulaut (Bucharest: INOE) p 35